# Fermilab

## Qudit Gate Decomposition Dependence for Lattice Gauge Theories

# Qudit Gate Decomposition Dependence for Lattice Gauge Theories

Doğa Murat Kürkçüoğlu,[1, 2, *] Henry Lamm,[1, 2, †] and Andrea Maestri[3, ‡]

[1]*Superconducting and Quantum Materials System Center (SQMS), Batavia, Illinois, 60510, USA.*
[2]*Fermi National Accelerator Laboratory, Batavia, Illinois, 60510, USA*
[3]*University of Amsterdam, 1090 GL Amsterdam, The Netherlands*
(Dated: October 23, 2024)

In this work, we investigate the effect of decomposition basis on primitive qudit gates on superconducting radio-frequency cavity-based quantum computers with applications to lattice gauge theory. Three approaches are tested: SNAP & Displacement gates, ECD & single-qubit rotations $R(\theta, \phi)$, and optimal pulse control. For all three decompositions, implementing the necessary sequence of rotations concurrently rather then sequentially can reduce the primitive gate run time. The number of blocks required for the faster ECD & $R_p(\theta)$ is found to scale $\mathcal{O}(d^2)$, while slower SNAP & Displacement set scales at worst $\mathcal{O}(d)$. For qudits with $d < 10$, the resulting gate times for the decompositions is similar, but strongly-dependent on experimental design choices. Optimal control can outperforms both decompositions for small $d$ by a factor of 2-12 at the cost of higher classical resources. Lastly, we find that SNAP & Displacement are slightly more robust to a simplified noise model.

## I. INTRODUCTION

While the advent of quantum computers offers the opportunity to investigate new questions in lattice gauge theories (LGT) [1–4], at present the gate resources are prohibitively large [5, 6]. Due to the large local Hilbert space of gauge theories, $d$-dimensional qudit-based computers can reduce the resources required [5, 7–14]. The potential algorithmic advantage of qudit platforms arises from the increased effective connectivity as native single-qudit $SU(d)$ rotations replace otherwise require non-local multi-qubit circuits [15–17]. In practice, this may allow for lower individual gate fidelities for the same algorithmic fidelity. Today, many promising systems for qudits are being explored including trapped ions [18–20], transmons [21–26], Rydberg arrays [27, 28], photonic circuits [29], ultra-cold atomic mixture [30], and superconducting radio frequency (SRF) cavities [31]. In this work, we focus on 3D superconducting radio-frequency (SRF) cavities derived from accelerator physics which possess decoherence times on the order of milliseconds [31]. Similar to qubits the possible gate sets are numerous; both for native gates [32–35] and fault-tolerant computation [36–46].

Quantum algorithms for lattice gauge theories generally require a set of fundamental group theoretic operations [47]. The identification of primitive subroutines divides the problem of formulating quantum algorithms for LGT into deriving said group-dependent primitives [5, 48–53] and group-independent algorithmic design [14, 50, 54–58]. In addition to the group dependence, the primitive subroutines vary based on the digitization of the gauge degrees of freedom. Some digitize in the representation basis with a maximum representation encoded [11, 13, 59–74]. Alternatively, the $q$-deformed formulation obtains

a finite dimensional Hilbert space by changing the symmetry group to be a so-called quantum group [14, 50]. Other formulations consider truncations within the bases of gauge-invariant states [75–83]. Further methods begin with different formulations or perform different approximations exist such as light-front quantization [84–86], conformal truncation [87], strong-coupling and large-$N_c$ expansions [88, 89]. Another approach is to formulate an inherently finite-dimensional Hilbert space theory with continuous local gauge symmetry which is in the same universality class as the original theory. Some methods for this include fuzzy gauge theories which use non-commutative geometry [90], and quantum link models which use rishons and an ancillary dimension [91–101].

In this work, we consider gates that arise naturally when digitizing with the discrete subgroup approximation [12, 52, 58, 75, 102–115]. The discrete group approximation has advantages over the methods discussed above. It is a finite mapping of group elements to integers that preserves a group structure; therefore reducing the amount of fixed- or floating-point quantum arithmetic, simplifying the primitive gates. This method has its roots in early Euclidean LGT where the discrete group structure allowed for reduction of the classical resources [116–122] and has seen a resurgence in the era of quantum computation [105, 106, 108, 123–125]. While the discrete subgroups are an approximation, they are related to the continuous groups broken by a Higgs mechanism [126–130] with work ongoing to understand this systematically [131].

At present, most work has emphasized qubit devices, but recent demonstrations of multi-qudit gates, have increased interest in qudit-based digitization methods [7–9, 11–14, 53]. Given the abundance of platforms and native gates, it would be valuable to explore the relative merits of different gate sets with respect to algorithmic implementation. Qudit-based SRF architectures are one such platform, and we explore prototype gates required for the simulation of LGT within the discrete subgroup approximation on them here. Focus is given to implementations on $d = 4, 6, 8$ states – respectively referred to

* dogak@fnal.gov
† hlamm@fnal.gov
‡ andreamaestrimaestri@gmail.com

as *ququart*, *quhexit*, and *quoctit*. We consider both state preparation and gates decomposed in three ways: SNAP & Displacement (S+D) gates, the echoed conditional displacement (ECD) & single-qubit rotation gates $R(\theta, \phi)$, and optimal pulse control. Comparisons between the three are made in terms of number of blocks, time-scales, and noise resilience.

This paper is organized as follows. A brief review of the field theory motivations and the general protocols we are interested in are found in Sec. II. In Sec. III, we briefly summarize the theory behind coupling a cavity to a two-level system to produce a qudit. This is followed in Sec. IV with a discussion about how the interacting Hamiltonian is used to implement digital gates and the three decompositions. Sec. V is where we describe the methods for determining our gate decompositions, the results of which are found in Sec. VI including an initial study of robustness to noise. We conclude in Sec. VII with summary and future work.

## II. LATTICE GAUGE THEORY

The gauge symmetries of particle physics constraint the possible interactions of theories, and thus only a finite set of gauge-group dependent primitive gates are required for simulation [47, 103]. These correspond to operations that can be performed on either one or two elements $g, h$ of the group $G$ stored in registers $|g\rangle, |h\rangle$. For the case of pure gauge theory (theories without the matter), the set of primitive gates are: the inverse gate $\mathfrak{U}_{-1}$ which sends a group element to its inverse:

$$\mathfrak{U}_{-1} |g\rangle = |g^{-1}\rangle; \tag{1}$$

the multiplication gate $\mathfrak{U}_\times$ that acts on two registers, changing the target to the left product with the control:

$$\mathfrak{U}_\times |g\rangle |h\rangle = |g\rangle |gh\rangle; \tag{2}$$

the trace gate $\mathfrak{U}_{\text{Tr}}$ which rotates $|g\rangle$ by a phase dependent on the trace of $g$ in a specified representation:

$$\mathfrak{U}_{\text{Tr}} |g\rangle = e^{i\theta \, Re \, Tr(g)} |g\rangle; \tag{3}$$

and the group Fourier transform $\mathfrak{U}_{FT}$ which acts on a single register with some amplitudes $f(g)$:

$$\mathfrak{U}_F \sum_{g \in G} f(g) |g\rangle = \sum_{\rho \in \hat{G}} \hat{f}(\rho)_{ij} |\rho, i, j\rangle. \tag{4}$$

The second sum is over $\rho$, the irreducible representations of $G$; $\hat{f}$ denotes the $G$ Fourier transform of $f$,

$$\hat{f}(\rho) = \sqrt{\frac{d_\rho}{|G|}} \sum_{g \in G} f(g)\rho(g), \tag{5}$$

where $|G|$ is the group size, $d_\rho$ is the dimensionality of the representation $\rho$, and $f$ is a function over $G$.
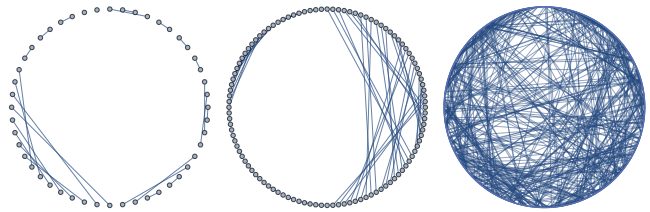


FIG. 1. Permutation graph necessary for implementing $\mathfrak{U}_{-1}$ for different discrete group: (left) the 48 element $\mathbb{BO}$, (center) the 108 element $\Sigma 108$, (right) the 1080 element $\Sigma(1080)$.

Because these operations act on at most two registers, they can be analyzed and optimized more efficiently than working at the algorithmic level; something dramatically demonstrated for $\mathfrak{U}_{FT}$ in a recent work [53]. Further, while $|G|$ (and therefore the optimal qudit dimension $d$) in the discrete subgroup approximation range from 24 to 1080, groups share structures which allows us to explore smaller gates while still being informative about preferred gate sets for HEP.

By inspecting Eq. (1), we recognize that $\mathfrak{U}_{-1}$ corresponds to a pair-wise permutation gate $|g\rangle \leftrightarrow |g^{-1}\rangle$ (See Fig. 1 for three example groups). If the qudit $d = |G|$, this gate is formed by a tensor product of at most $|G|/2$ Pauli $X^{(g,h)}$ gates between states $|g\rangle, |h\rangle$. An example of this for the 24 element $\mathbb{BT}$ mapped to a quicosotetrit ($d = 24$ qudit) is shown in the top of Fig. 2. As such, universal gate sets that can perform multiple $X^{(g,h)}$ concurrently would yield algorithmic improvement. If $d < |G|$, the gate structure generalizes from $X^{(g,h)}$ gates to requiring controlled permutations that couple the qudits. Another important structure exemplified in Fig. (1) is that the maximum distance between $|g\rangle$ and $|g^{-1}\rangle$ is $\sim \frac{1}{2}|G|$ – another way to discriminate the efficiency of gate sets.

The only two-register gate, $\mathfrak{U}_\times$, corresponds to a controlled permutation gate where a different permutation gate is applied depending on the control qudit state. As such, it has similar implementation requirements to $\mathfrak{U}_{-1}$. Further, $\mathfrak{U}_{\text{Tr}}$ is diagonal in state space. Therefore if $d = |G|$, the only elementary gate required is $R_Z^{(g,h)}(\theta)$ which generates a $R_Z$ gate of phase $\theta$ between $|g\rangle$ and $|h\rangle$ (See the bottom of Fig. 2).

The final gate, $\mathfrak{U}_F$, can be decomposed for $d = |G|$ into a tensor product of $SU(|\mathcal{C}|)$ rotations $\mathcal{U}_N^{(a,b...,n)}$ where the size of set $\{\mathcal{C}\}$ is the order of the conjugacy class $\mathcal{C}$ of the group [49]. For $d < |G|$, these must be mapped to controlled $SU(N)$ gates. Although the spacing between states $a, b \ldots, n$ could in principle be $\sim |G|$, we find that for the discrete subgroup approximation, $|\mathcal{C}| \lesssim \sqrt{|G|}$ with the maximum $|\mathcal{C}| = 18$. The smallest possible rotation is $SU(2)$, where the Euler angle decomposition can be built from an ZXZ rotation where the superscripts indicate levels that are rotated:

$$\mathcal{U}_2^{(a,b)}(\vec{\theta}) = R_Z^{(a,b)}(\theta_0) R_X^{(a,b)}(\theta_1) R_Z^{(a,b)}(\theta_2). \tag{6}$$

We can combine $\mathcal{U}_N^{(a,b...,n)}$ for the conjugacy class $\mathcal{C}$ into

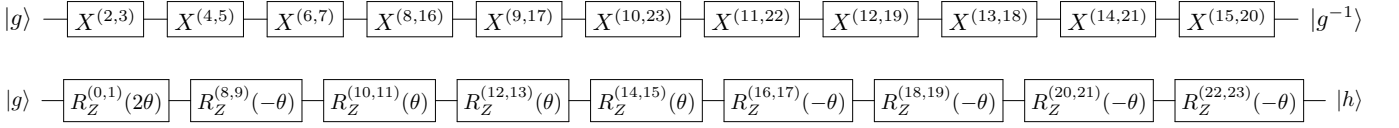FIG. 2. Implementation of $\mathbb{BT}$ primitive gate assuming a quicosotetrit: (top) $\mathfrak{U}_{-1}$ (bottom) $\mathfrak{U}_{\mathrm{Tr}}$. Note for the inverse gate the largest distance between a $|g\rangle$ and $|g^{-1}\rangle$ is 13

an operator $V_{\mathcal{C}}$. For example, one conjugacy class with order 2 in $\mathbb{BT}$ yields [49]:

$$V_1 = \prod_{a=0}^{11} \mathcal{U}_2^{(2a,2a+1)}(\vec{\theta}). \qquad (7)$$

$V_{\mathcal{C}}$ for larger $n$ are constructed recursively with additional Givens rotations [132–135]. $SU(3)$ rotations requires

$$\mathcal{U}_3^{(a,b,c)}(\vec{\theta}) = \mathcal{U}_2^{(a,b)}(\vec{\theta_0}) R_X^{(b,c)}(\theta_1) \mathcal{U}_2^{(a,b)}(\vec{\theta_2}) R_Z^{(b,c)}(\theta_3). \qquad (8)$$

while an $SU(6)$ needs from two $\mathcal{U}_3^{(a,b,c)}(\vec{\theta})$ and three $\mathcal{U}_2^{(a,b)}(\vec{\phi})$ (where we suppress the arguments below):

$$\mathcal{U}_6^{(a,b,c,d,e,f)} = \mathcal{U}_3^{(a,b,c)} \mathcal{U}_3^{(d,e,f)} \mathcal{U}_2^{(a,d)} \mathcal{U}_2^{(b,e)} \mathcal{U}_2^{(c,f)}. \qquad (9)$$

With these, a $V_{\mathcal{C}}$ with order 6 for $\mathbb{BT}$ is

$$\begin{aligned} V_9 = &\mathcal{U}_6^{(0,9,16,1,8,17)} \mathcal{U}_6^{(2,14,20,3,15,21)} \\ &\mathcal{U}_6^{(4,11,23,5,10,22)} \mathcal{U}_6^{(6,12,19,7,13,18)}. \end{aligned} \qquad (10)$$

Thus, $\mathfrak{U}_{\mathrm{F}}$ is a tensor product of a few $SU(N < 18)$ rotations between well-separated qudit states.

Along with primitive gates, the opportunity for optimizing state preparation in LGT should be considered. In situations where gauge redundant encodings are necessary, one often prepares a gauge-dependent state and then applies a gauge-symmetrization operator. This gate acts as a projection operator [47, 58, 103, 136]:

$$\begin{aligned} P |U_{ij} \ldots\rangle &= \frac{1}{|G|^N} \left( \int_G \mathrm{d}g_1 \int_G \mathrm{d}g_2 \ldots \right) \left| g_2 U_{ij} g_1^\dagger \ldots \right\rangle \\ &= \frac{1}{|G|^N} \int_{G^N} \mathrm{d}g \, \phi(g) |U\rangle. \end{aligned} \qquad (11)$$

The structure of this operator is a sum over $\mathfrak{U}_\times$, and thus again a set of controlled permutation matrices. This constraint allows one to restrict the possible state that must be initially prepared, simplifying state preparation optimization. Further, algorithmic choices in state preparation can simplify the possible initial states [114, 137, 138].

To summarize, the general structures of a LGT primitive gates are tensor products of $X^{(a,b)}$ and $SU(N < |G|)$ rotations between states that are typically well-separated. While it could prove experimentally hard to create qudits with $d = |G|$, for smaller $d$ the single register gates become similar to the controlled-permutations required for $\mathfrak{U}_\times$, so one can start with considering how prototype gates on smaller qudits can be compiled.

## III. 3D CAVITY QED

The hardware platform we will study here corresponds to an SRF cavity mode (qumode) coupled to a two level system (qubit). With $\hbar = 1$, a simplistic model of this interaction from circuit QED is the *Jaynes-Cummings model* [139]:

$$H = \omega_c \hat{a}^\dagger \hat{a} + \frac{1}{2}\omega_0 \sigma_z + g(\hat{a}^\dagger \sigma_- + \hat{a}\sigma_+). \qquad (12)$$

where $\omega_c$ is the frequency of the qumode with creation and annihilation operators $\hat{a}, \hat{a}^\dagger$, $\omega_0$ is the frequency of the two-level system which is acted on by the Pauli operators $\sigma_i$, and $g$ is a coupling between the qumode and qubit. The regime considered, particularly amenable to hardware, is the so-called dispersive regime, which occurs when $\Delta = |\omega_0 - \omega_c| \gg g$ [140]. In this regime, one can approximately diagonalize $H$ using a unitary transformation $D^\dagger H D$ with

$$D = e^{\lambda(\hat{a}^\dagger \sigma_- - \hat{a}\sigma_+)} \qquad (13)$$

where $\lambda = g/\Delta$. By doing so, and expanding to $\mathcal{O}(\lambda)$, one obtains

$$H = \omega_c \hat{a}^\dagger \hat{a} + \frac{1}{2}\omega_q \sigma_z + \frac{1}{2}\chi \hat{a}^\dagger \hat{a}\sigma_z + \mathcal{O}(\lambda^2), \qquad (14)$$

where $\chi = 2g\lambda = 2g^2/\Delta$ is called the dispersive shift and $\omega_q = \omega_0 + \chi$. With this, the Fock states of the qumode ($|0\rangle, |1\rangle, |2\rangle \ldots$) can be used as a qudit computational space, and the ancilla qubit provides an interaction to manipulate the qudit.

An easy way to control the system is to add additional fields acting on the qumode and the qubit. A possible choice is to add a single control on both:

$$\begin{aligned} H = &\omega_c \hat{a}^\dagger \hat{a} + \frac{1}{2}\omega_q \sigma_z + \chi \hat{a}^\dagger \hat{a}\sigma_z \\ &+ \epsilon(t)\hat{a}^\dagger + \epsilon(t)^* \hat{a} + \Omega(t)\sigma_+ + \Omega(t)^* \sigma_-. \end{aligned} \qquad (15)$$

which we define as $H = H_0 + H_1$ as a non-interacting $H_0 = \omega_c \hat{a}^\dagger \hat{a} + \frac{1}{2}\omega_q \sigma_z$, and the remaining terms the interacting Hamiltonian $H_1$.

With this choice of controls and enough time, it is possible to manipulate the system to reach any arbitrary state [141]. It is important to emphasise that for SRF cavities there is not an agreed-upon mode of operation. Therefore, the investigation of different gate sets [32–35] and optimal control [141–149], is key to fully exploit these systems. At a higher level of abstraction, performing efficient compilation of quantum circuits to qudits rather the qubits also requires new techniques [5, 150–154].

## IV. GATE IMPLEMENTATION

To obtain a theoretical target gate $U_t$, one manipulates the time-dependent couplings of Eq. (15). All approaches require this optimization at the Hamiltonian level, and in this section we summarize two ways to do so. The first approach only relies on direct optimization of $\epsilon(t), \Omega(t)$, while the other decomposes $U_t$ into a set of simpler gates that have been optimized at the Hamiltonian level. In either case, one considers a quantum state $|\psi(t)\rangle$ evolving according to the Schrödinger equation with a particular time-dependent Hamiltonian $H(t)$. This state can be approximated by dividing $t$ into time steps of size $\delta t$:

$$|\psi(t)\rangle \approx \prod_{n=0}^{t/\delta t} e^{-iH(n\delta t)\delta t} |\psi(0)\rangle \equiv V |\psi(0)\rangle, \quad (16)$$

with increasing accuracy as $\delta t \to 0$.

Clearly, $H(t)$ allows transition between quantum states, and thus $V$ correspond to a digital quantum circuit. The goal is then is to find a $V$ which implements $U_t$ with high fidelity. It is important to emphasise that $V$ as defined in Eq. (16) makes reference to a state $|\psi(0)\rangle$. It is the case that the state-dependent fidelities vary substantially [155–157] and therefore synthesizing a general unitary is harder than preparing a state from a given $|\psi(0)\rangle$. Proceeding, we will distinguish between gates for *state preparation* which are optimized only for acting on vacuum $|0\rangle$, and general gates which should have high fidelity on any $|\psi(0)\rangle$.

To study these effects, we need to define the infidelity i.e. a cost function $\mathcal{I}(U_t, V)$ to minimize. Given that the goal is to implement a target gate $U_t$, a common approach consists of dividing the time into $N$ time steps and for each of these, the control pulses $\Omega(n\delta t), \epsilon(n\delta t)$ are constant. A main drawback of this approach is the increasing number of time steps – and therefore optimization parameters– required when increasing $d$ of the qudit [35, 141], this is because while the controls can generate the algebra, reaching higher states requires more and more commutators. Another drawback is the pulse discontinuities. By optimizing only the field amplitudes at each time step, we are neglecting the time required to ramp the fields on the physical hardware, which can introduce additional infidelity or must be implemented as expensive constraints on the optimization. Further, increasing $N$ requires more matrix multiplications in the optimization algorithm. Looking at Eq. (16), for a $d$-dimensional qudit $N$ matrix multiplications are required to compute the evolution of the system, leading to $\mathcal{O}(Nd^3)$ operations. Lastly, when optimizing the cost function, unless the optimization method is gradient-free, it is necessary to compute either the gradient or in some cases the hessian – further increases the complexity. For $N$ parameters, without recycling computations, the cost function needs to be evaluated $N + 1$ times, which leads to an overall complexity of $\mathcal{O}(N^2 d^3)$.

An alternative approach avoids piecewise constant terms and instead optimize gates in a different basis.

Looking at the expression of Eq. (15), a way to generate smooth pulses, making it easier to implement, is to expand them in some polynomial basis [158, 159], where the optimal choice can be problem-dependent. Moreover, the number of basis states directly controls how steep the pulse ramping can be. Here, we will expand in Chebyshev polynomials which provide an exact $n^{th}$ order interpolation function for any $n^{th}$ order polynomial. Approximating instead using the Fourier series requires more terms to reach a comparable accuracy [160]. Rewriting Eq. (15) in the Chebyshev basis of $T_k(t)$, yields

$$H = H_0 + \chi \hat{a}^\dagger \hat{a} \sigma_z + \sum_{k=0}^{N} \left[ (c_k \hat{a}^\dagger + q_k \sigma_+) T_k(t) + h.c. \right], \quad (17)$$

where $\{c_k\}$ and $\{q_k\}$ are the coefficients of the qumode and the qubit, respectively. Using this expression for $H$, it is possible to compute the $V$. Its magnitude depends on the dimension of the cavity space that is optimized, the duration of the pulses, and on the resolution of the hardware on which the pulses are optimized.

### A. Interaction picture

Finding an optimal $V$ from Eq. (17) can be made easier by transforming into the interaction frame of reference [161]. Since $H_0$ is time-independent, the time-evolution can be solved analytically:

$$U_0(t) = e^{-iH_0 t}.$$

With this expression, it is possible to define a state vector in this new frame of reference:

$$|\psi_I(t)\rangle = U_0(t) |\psi_S(t)\rangle, \quad (18)$$

where $|\psi_S(t)\rangle$ represents the state governed by Schrodinger equation. Using this, it is possible to write

$$i\frac{\partial}{\partial t} |\psi_S(t)\rangle = H |\psi_S(t)\rangle = e^{-iH_0 t} \left( H_0 + i\frac{\partial}{\partial t} \right) |\psi_I(t)\rangle$$

$$\implies i\frac{\partial}{\partial t} |\psi_I(t)\rangle = e^{iH_0 t} H_1 e^{-iH_0 t} |\psi_I(t)\rangle. \quad (19)$$

This can be used to simplified optimization of $V$ by solving Eq. (19) and then transforming back to the initial frame by multiplying by the inverse transformation defined by Eq. (18). The remaining step consists in writing explicitly the term that dictates the evolution of the system:

$$H_{1_I} = e^{iH_0 t} H_1 e^{-iH_0 t}$$

with the resulting operator being

$$H_{1_I} = \chi \hat{a}^\dagger \hat{a} \sigma_z + \sum_{k=0}^{N} [c_k C_k(t) \hat{a}^\dagger + q_k Q_k(t) \sigma_+ + h.c]. \quad (20)$$

where

$$C_k(t) \equiv T_k(t)e^{i\omega_c t}$$
$$Q_k(t) \equiv T_k(t)e^{i\omega_q t},$$

While optimizing the pulses in the interaction picture may be easier, the pulses must be converted back to the laboratory frame by multiplying them with the exponential factors that are missing in Eq. (20). This may reduce accuracy, depending on the hardware precision.

To inform the gate synthesis that is developed in this work, it is important to give some realistic near-term properties for 3D cavities. We take for a fiducial decoherence time of the cavity $T_1 = 10\ ms$ [162]. With this, we take $\omega_c = 5$ GHz, $\omega_q = 3$ GHz, and $\chi = 0.3$ MHz. Regarding the control pulses, we consider a max time resolution of 1 ns (corresponding to 1 giga-sample/$s$) for the state preparation, and a longer 10ns time resolution for the pulses used for gate optimization. An additional constraint is for the drive amplitudes to change by no more than a 1 MHz/$ns$ (to maintain a smooth drive profile) which is consistent with near-term SRF cavities.

## B. Gate decomposition in universal sets

One could imagine engineering an optimized pulse for each LGT primitive, although issues with computational expense and error correction may complicate this. Instead, one might decompose each primitive into a limited set of universal gates whose implementation is known at the Hamiltonian level with high fidelity. The price of this is increased runtime of the primitive. While qudits can decrease the circuit depth for LGT [49], improvements are gate-set dependent. Thus we consider two universal sets: SNAP & Displacement and ECD.

### 1. SNAP & Displacement

The qudit gate set of SNAP and Displacement gates ($S+D$) has been widely discussed in the literature [32–34, 150] and we briefly review the key points here. Crucially, the universality of $S + D$ is known [141]. The Displacement gate is produced by driving the cavity on resonance with a calibrated pulse of a specific amplitude and length. It can be expressed as

$$D(\alpha) = e^{(\alpha\hat{a}^\dagger - \alpha^*\hat{a})}, \qquad (21)$$

and generates a coherent state $|\alpha\rangle$ from the vacuum displaced in phase space by $\alpha$ i.e. $D(\alpha)|0\rangle = |\alpha\rangle$. An important property of $D(\alpha)$ is that its Hermitian conjugate $D^\dagger(\alpha) = D(-\alpha)$. The parameter $\alpha$ of Eq. (21) can be considered real, without loss of generality. Mathematically $D(\alpha)$ represents the Heisenberg group which may prove useful for compilation. For reasonable $\chi$ on GHz SRF cavities with $T_1, T_2 \sim \mathcal{O}(1)$ ms, the gate times range from $0.01 - 0.2$ $\mu$s depending on $\alpha$ [163].

The SNAP gate applies arbitrary phases to Fock states

$$S(\vec{\theta}) = \sum_{k=0}^{d-1} e^{i\theta_k} |k\rangle \langle k|. \qquad (22)$$

This is produced by driving the qubit with $\pi$ pulses with relative phases, which cause a phase kick-back onto the qudit. Importantly, while the qubit is used to implement this gate, upon completion the qubit is unentangled from the qudit. To ensure high fidelity, the driving strength for a SNAP must be taken $\max(Q_k(t)) \ll \chi$, with a good heuristic found to be a pulse length of $\pi/(10\chi)$. While larger $\chi$ allows for faster SNAP gates, the need to avoid strong self-Kerr interactions limits its size. Reasonable values for $\chi$ for GHz cavities with $T_1, T_2 \sim 1$ ms lead to SNAP gate times between $1 - 50$ $\mu$s [31, 35, 162].

With these, any single-qudit gate can be approximately decomposed by [33]:

$$U_t = \left(\prod_{k=0}^{M} D(\alpha_k)S(\vec{\theta}_k)\right) D(\alpha_{M+1}), \qquad (23)$$

where $B$ is the number of blocks used. For a $d$-state qudit, an $B$ block decomposition has $(d+1)B+1$ free parameters. Since an arbitrary qudit state can be obtained by an $SU(d)$ rotation with $d^2 - 1$ parameters, a naive estimate for the decomposition of any single qudit state is at most $B = \frac{d^2-2}{d+1} \sim \mathcal{O}(d)$ [164]. This represented an algorithmic improvement over the $\mathcal{O}(d^2)$ scaling of a $\log_2(d)$ qubit device with access to only one and two-qubit gates [17]. The authors of [33] empirically found that a broad set of qudit gates (with $d \leq 10$) can be decomposed according to Eq. (23) with only 3 to 4 blocks and that the fidelity $\mathcal{F} \approx 1 - e^{-6.49(B/d)^{1.91}}$.

Following the LGT insight discussed in Sec. II that permutation matrices represent a sizeable fraction of the primitives necessary, we investigated whether these gates represent a special subset of all qudit gates in terms of their fidelity under $S + D$ decomposition. For all d! permutation gates with d = [3, 6] we performed 10 decompositions with $B = [1, 6]$, where the parameters for the decompositions were randomly initialized. From this data, the best fit to the functional form advocated in [33] was $\mathcal{F}_{\text{perm}} \approx 1 - e^{-3.8(5)(B/d)^{0.5(1)}}$. This dependence shows that for values of $B/d \lesssim 1$, permutation gates can be decomposed with higher fidelity than general gates. In Fig. 3 we present the distribution of permutation gate fidelities for $d = 6$ as a function of M. From the figure, one observes a clear bimodal distribution in $\mathcal{F}$ for $B = 3, 6$. Beyond finding that permutation gates are easier to decompose than general $SU(d)$ matrices, one could ask if specific permutation decompositions are better – especially in light of the bimodal distribution. Given the freedom in encoding of LGT, such algorithmic input could be used similar to Gray codes on qubits to reduce noise or gates [165–168]. As such, we investigated the dependence of $\mathcal{F}$ for $d = 6$ permutation gates on two distance metrics
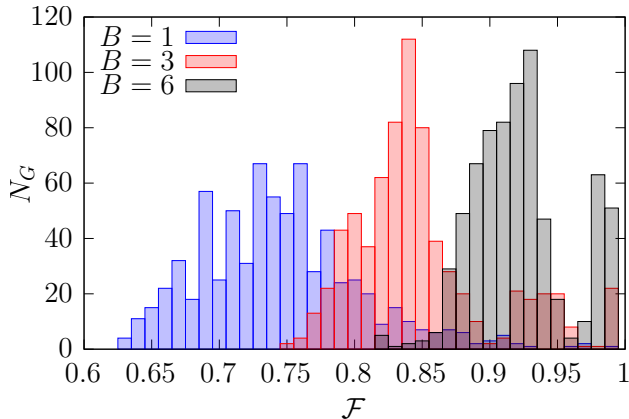
FIG. 3. Number of $d = 6$ permutation gates $N_G$ with given fidelity as a function of $B$ for $S + D$.

used for distinguishing between strings when we write the permutations as tuples, for example

$$\begin{pmatrix} 0 & 1 & 0 \\ 1 & 0 & 0 \\ 0 & 0 & 1 \end{pmatrix} \rightarrow (1, 0, 2). \qquad (24)$$

where the $i$−th entry $j$ of the tuple corresponds to permuting the state $|j\rangle \rightarrow |i\rangle$. The first is the *Kendall rank correlation coefficient* $K_C$ which is used as a statistic measure between two sets of data $x = \{x_0 \ldots x_n\}$ and $y = \{y_0 \ldots y_n\}$ of their relative monotonicity [169]. It is defined in terms of the number of pairs $(x_i, y_i)$ and $(x_j, y_j)$ that are concordant, i.e. for $i < j$ either $x_i < x_j$ and $y_i < y_j$ or $x_i > x_j$ and $y_i > y_j$. If we call this number $n_c$, and the remaining discordant pairs $n_d$ then $K_C$ is

$$K_C = \frac{n_c - n_d}{n_c + n_d} \qquad (25)$$

where $K_C$ can range from 1 when the two sets are identical to -1 when the two sets are exactly reverse. We take $x = (0, 1 \ldots, d) = \mathbb{1}_d$, and thus $K_C$ is measured from it. The results are found in Fig. 4. From these it is clear that $K_C$ does capture some of the dependence of $\mathcal{F}$ on permutation, with higher $K_C$ typically having larger $\mathcal{F}$. In particular we see that the bimodal distribution of Fig. 3 is correlated with positive $K_C$. Investigating further, one observes that $\mathcal{F}(K_C)$ is non-monotonic, reaching a minimum at $K_C = 0$ with a large variance, before rising slightly toward $K_C \rightarrow -1$.

Another metric for comparing sets, with its origin in spell checking, is the *Damerau–Levenshtein distance* [170, 171] $D_{\text{perm}}$ which here counts only the number of transposition of two adjacent characters required to change one word into another. Fig. 5 presents $\mathcal{F}$ as a function of $D_{\text{perm}}$. We do observe decreasing $\mathcal{F}$ with $D_{\text{perm}}$. From the best fit lines in Fig 5, we see that $1 - \mathcal{F} \approx [10^{-3}, 10^{-2}]D_{\text{perm}}$ with some weak quadratic term. With this, one can make a comparison between
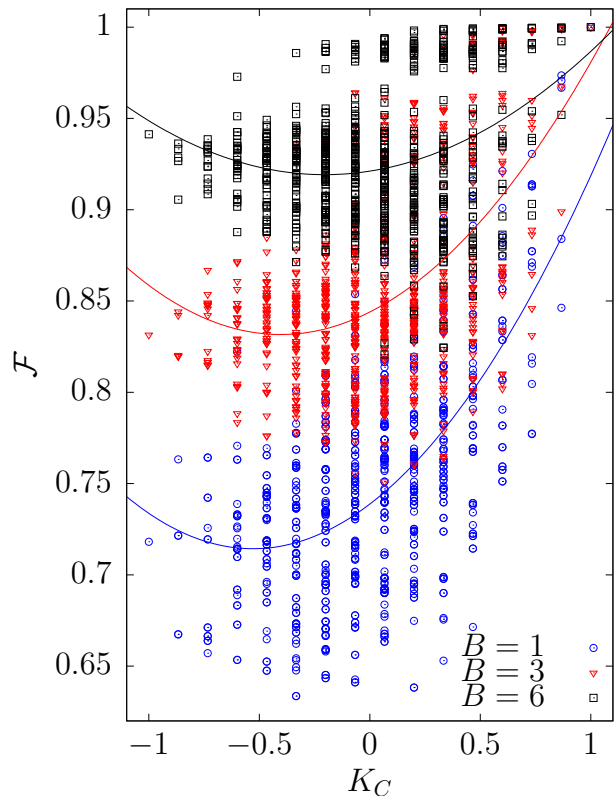


FIG. 4. Fidelity of $d = 6$ permutation gates vs. $K_C$ and $B$. Quadratic best fit lines are shown to guide the eye.

directly decomposing a gate with and decomposing in terms of $N = D_{perm}$ single $X^{(a,a+1)}$ with smaller $B$ each with individual $\mathcal{F}_{ind}$. In the best case for the single gates,

$$1 - 10^{-2} D_{\text{perm}} = \mathcal{F}_{ind}^{D_{\text{perm}}} \implies F_{ind} > 0.990 \qquad (26)$$

Since this high fidelity for $B < D_{perm}$ decomposing directly into $S + D$ is always more efficient.

Taken together, we conclude that permutation gates represent an important subset of gates under $S + D$ decomposition with higher than average fidelity. Further, specific classes of permutation gates appear to have still better scaling and thus could be useful in optimizing digitization of LGT.

### 2. ECD decomposition

One limitation of S + D is that operations require time comparable to $2\pi/\chi$. This is a limiting factor in the weak-dispersive regime because decoherence will reduce fidelity. To overcome this challenge, another universal set has been proposed which combines an echoed conditional displacement $ECD$ gate with single qubit rotations [35]:

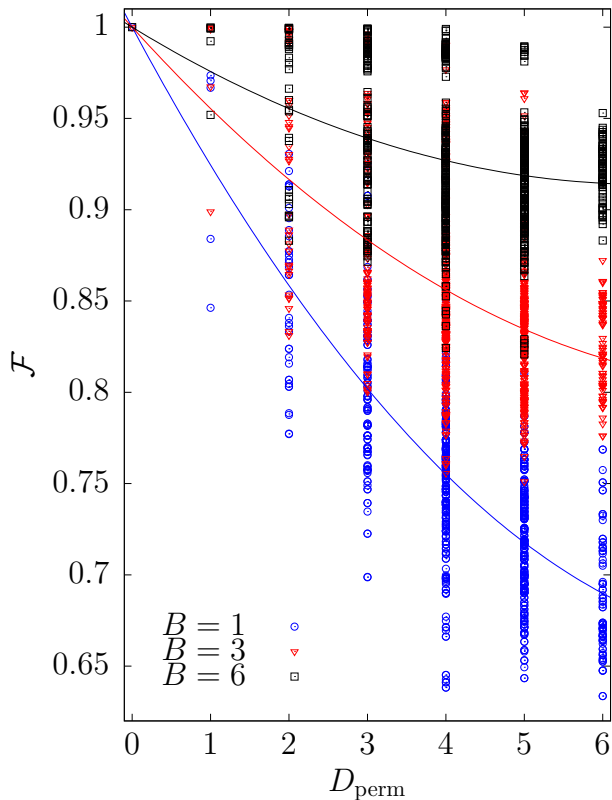$$U_t = \left( \prod_{k=0}^{M} R(\theta_k, \phi_k) ECD(\alpha_k) \right) R(\theta_M, \phi_M), \qquad (27)$$

FIG. 5. Fidelity of $d = 6$ permutation gates vs. $D_{\text{perm}}$ for different block sizes $B$. Quadratic best fit lines with $\mathcal{F}(0) = 1$ are shown to guide the eye.

where the ECD gate corresponds to applying $D$ gates conditioned on the state of the qubit,

$$ECD(\alpha) = D(\alpha/2) |e\rangle \langle g| + D(-\alpha/2) |g\rangle \langle e| .$$

To enable universality, this is coupled to unselective qubit rotation

$$R(\theta, \phi) = \exp\left( -\frac{i\theta}{2} (\sigma_x \cos \phi + \sigma_y \sin \phi) \right).$$

In constrast to S+D, only the *ECD* gate acts directly on the qudit. In this scheme $R(\theta, \phi)$ acts on the qubit changing the relative displacement. As such, the qubit and qudit may still be entangled at the end of a block. This leads to greater sensitivity of the qudit to noise from the qubit. Modern transmon qubits can perform $R(\theta, \phi)$ in $\mathcal{O}(0.01\ \mu\text{s})$. $ECD(\alpha)$ can be implemented in $T \propto \frac{\alpha}{\chi \alpha_0}$ where $\alpha_0$ is the magnitude of the intermediate oscillator displacement. For GHz cavities and reasonable values of $\alpha_0 \sim 30$ this would correspond to $0.1 - 0.5\ \mu\text{s}$ [31, 35].

Counting parameters, $B$ blocks have $3B + 2$. Since the qubit may not be decoupled, the general state is given by an $SU(2d)$ rotation with $4d^2 - 1$ parameters. This naively estimates that $\frac{4}{3}d^2 - 1$ blocks are needed – $\mathcal{O}(d^2)$ scaling – which is parametrically worse that $S + D$. As will be seen below, this larger $B$ can be compensated by the faster gate times.

One should also compare to State-of-the-art qubit implementations, which also scale asymptotically as $\mathcal{O}(d^2)$. An $SU(2^n)$ unitary where $d = 2^n$ requires [17] a number of sequential CNOTs

$$N_{\text{CNOT}} = \frac{21}{16}d^2 - d - \frac{3}{4}d \log_2(d) \tag{28}$$

which suggests a comparable circuit depth to *ECD*. Further, the theoretical lower bound is $N_{\text{CNOT}} = \frac{1}{4}[d^2 - 1 - 3 \log_2(d)]$ [172] while the lower bound on *ECD* is unknown. Importantly, modern transmon-based platforms can perform CNOT gates in $\sim 0.5\ \mu s$ [173], similar to the higher estimates for near-term ECD gates. Taken together, these results suggest that the algorithmic advantage of qudit-based platforms with ECD gate sets over qubit devices depends upon acheiving gate times below $0.5\ \mu s$ and clearer decomposition estimates.

## V.  METHODS

For optimization, we have used `LBFGS` as our optimization algorithm [174]. For preparing $|\Psi\rangle$, one solves the pulse optimization of Eq. (16) using the parameters in Eq. (17) with a fixed $|\psi(0)\rangle$. For general gate preparation, the more complicated optimization procedure motivates using the interaction picture of Eq. (20). Further, given the larger number of optimization parameters, we found efficiency gains from first optimizing pulses with a small number of coefficients, and then growing the bases while using as initial conditions for the next iterations the previous results[1] In order to compare the optimized gates with the target, it is necessary to define a cost function. In the literature, there is a number considered, typically related to $p$ norms [32, 33, 35, 49, 141, 143, 145, 147]:

$$||A||_p = \sup_{x \neq 0} \frac{||Ax||_p}{||x||_p} \tag{29}$$

which use the $p$ vector norm,

$$||x||_p = \left( \sum_i |x_i|^p \right)^{1/p} . \tag{30}$$

If the goal is preparing $|\Psi\rangle$, the optimization problem can be restricted to only a subspace of the full system. Here, we follow prior work and use as a cost function the infidelity:

$$\mathcal{I} = 1 - |\langle \Psi | V | \psi(0)\rangle|^2, \tag{31}$$

Typically, $|\psi(0)\rangle = |0\rangle$, but we will investigate a limited set of other initial states as a way to understand robustness of state preparation to noise.

––––––––––

[1] The entire parallelized codebase is written in `Julia` and can be found at https://github.com/AndreaMaestri18/Opt3DQalgs.
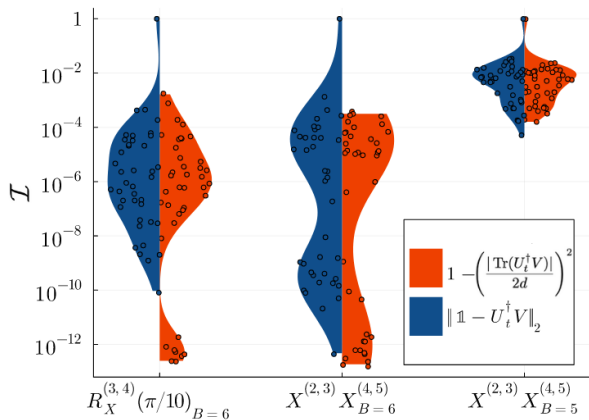
FIG. 6. Distribution of $\mathcal{I}$ of two cost functions for three gates on a quhexit using $S+D$ decomposition, after 30 optimizations and using different numbers of blocks $B$.

In case where we wish to optimize $V$ to approximate a gate $U_t$, one must account for working in the interacting picture by multiplying the target by the inverse of the transformation $U_0(T)$ defined in Eq. (18). With this, the most common cost function to minimize is :

$$\mathcal{I} = 1 - \left( \frac{|\operatorname{Tr}(U_t^\dagger U_0(T)V)|}{2d} \right)^2 \quad (32)$$

where $2d$ is the dimension of the combined cavity and qubit space. The idea behind this measure is that if $V \approx U_t$, using the properties of the unitary matrices we have $\mathcal{I} \longrightarrow 0$. Other options to measure the distance between 2 matrices could be:

$$\mathcal{I} = ||\mathbb{1} - U_t^\dagger U_0(T)V||_2. \quad (33)$$

which still relies on unitarity, and the norm of the difference between the matrices:

$$\mathcal{I} = ||U_t - U_0(T)V||_2. \quad (34)$$

## VI.   NUMERICAL RESULTS

In this section, we numerically optimize decompositions of a set of prototypical gates for HEP. As a first step, we studied how minimizing the different infidelities $\mathcal{I}$ of Eqs. (32), (34), and (33) as a cost function. This preliminary analysis was used to decide which cost function going forward. The cases considered were $S + D$ decomposition of two gates on a quhexit: a double $X$ gate, $X^{(2,3)}X^{(4,5)}$ (with two different block sizes) and $R_X^{(2,3)}(\pi/10)$ gate. While we tested the three norms, the results coming from the optimization of eq. (34) showed poor, slow convergence and thus in-depth analysis was done only on the remaining cost functions which are presented in Fig. 6. In this figure, we present the infidelity of trace-norm for both optimization functions eq. (33).
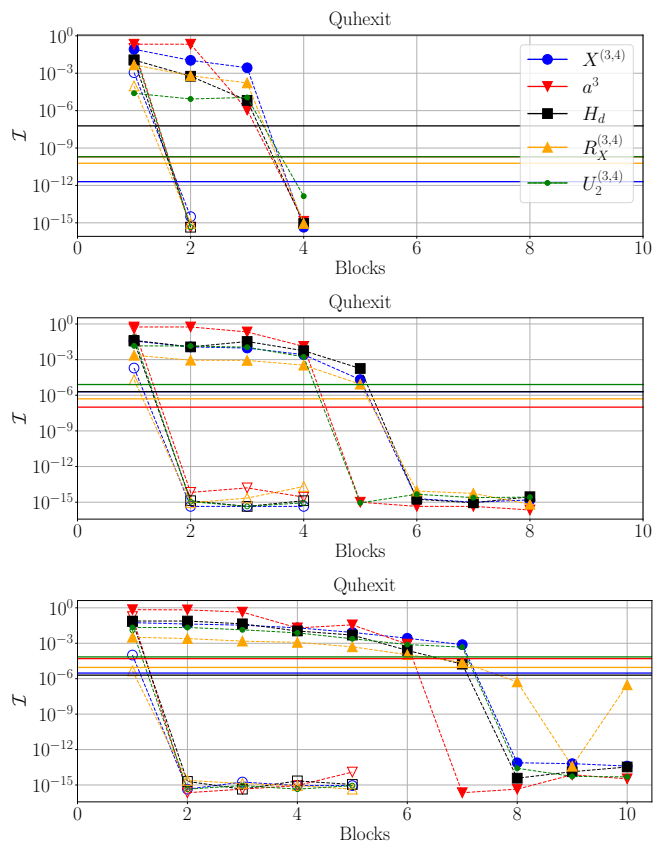


FIG. 7. $S + D$ (open points) and $ECD$ (closed points) decompositions of different state preparations for: (top) ququart, (middle) quhexit, (bottom) quoctit. The horizontal lines correspond to the reference values of the PO infidelities.

One observes from these results that varying cost function leads to different decompositions, with distinct distributions related to how the matrix elements are weighted. A more sophisticated two-sided t-test for unequal variances confirms this. Putting everything together, the trace distance defined in Eq. (32) generally produced lower $\mathcal{I}$. Therefore this metric will be used in what follows.

We now study preparation of the following states $|\Psi\rangle$ on all three qudits and using all three decompositions:

- Fock state 3: $a^3 |0\rangle = |3\rangle$, which is a representative of an electric basis state

- $d-$Hadamard state: $H_d |0\rangle = \frac{1}{\sqrt{d}} \sum_i |i\rangle$, which can be taken as a prototype of the weak-coupling gauge-invariant vacuum state in the magnetic basis

- $X^{(3,4)}$, $R_X^{(3,4)}(\pi/10)$, $U_2^{(3,4)}(\frac{\pi}{5}, \frac{2\pi}{15}, \frac{\pi}{10})$ applied to randomly-generated state: $|\psi_{ran}\rangle \rightarrow U_{target} |\psi_{ran}\rangle$, correspond to prototypes of general HEP states that are prepared on a potentially noisy device.

For each decomposition, $\mathcal{I}$ as a function of $B$ are presented in Fig. (7). From these $|\Psi\rangle$, the $S + D$ decompositions appear independent of qudit size $d-$ always requiring

TABLE I. $\mathcal{I}$ from pulse optimization of state preparation on different qudits.

| $d$ | T [$\mu$s] | $X$ | $R_X$ | $U_2$ | $|0\rangle \to |3\rangle$ | $|0\rangle \to |H\rangle$ |
|---|---|---|---|---|---|---|
| 4 | 0.1 | $2 \times 10^{-12}$ | $6 \times 10^{-11}$ | $2 \times 10^{-10}$ | $2 \times 10^{-10}$ | $6 \times 10^{-8}$ |
| 6 | 0.2 | $2 \times 10^{-6}$ | $5 \times 10^{-7}$ | $8 \times 10^{-6}$ | $1 \times 10^{-7}$ | $2 \times 10^{-6}$ |
| 8 | 0.5 | $3 \times 10^{-6}$ | $9 \times 10^{-6}$ | $7 \times 10^{-5}$ | $5 \times 10^{-5}$ | $2 \times 10^{-6}$ |

a block size $B_{S+D} = 2$ to reach $\mathcal{I} < 10^{-15}$. In contrast reaching $\mathcal{I} < 10^{-15}$ requires $B_{ECD} \approx d$. Thus these $|\Psi\rangle$ confirms the expectations of $B_{ECD} > B_{S+D}$ and the scaling from naive parameter counting. Further, while $ECD$ requires more blocks, the potential 2-50$\times$ faster time per block can mitigate this so the ultimate preference depends on experimental hardware. These results can be compared to pulse optimization with total times roughly one block of the ECD gate but different for each qudit: $T_{PO}^4 = 0.1 \ \mu s$, $T_{PO}^6 = 0.2 \mu s$. $T_{PO}^8 = 0.5 \ \mu s$. Example of the pulses for the quhexit are found in Fig. (7). While these pulses do not start and stop at zero power, imposing smooth ramping was found to have only small effect on $\mathcal{I}$ but greatly increased convergence time. From this, $\mathcal{I}_{PO} \lesssim 10^{-5}$ has a clear dependence on $d$.

Moving to gate decomposition, we consider the following gates which are prototypical of HEP primitives:

- $X^{(3,4)}$, $X^{(2,5)}$, and $X^{(2,3)}X^{(4,5)}$ which can be related to $\mathfrak{U}_{-1}$ and $\mathfrak{U}_{\times}$

- $R_X^{(3,4)}(\theta)$ with $\theta = \pi, \pi/5, \pi/10$ which model $\mathfrak{U}_{\text{Tr}}$ and $\mathfrak{U}_{\text{F}}$.

For these gates, we consider their decomposition on quhexits with $S + D$ and $ECD$ (See Fig. (9)). In contrast to state preparation, $\mathcal{I}$ depends strongly upon $B$. We observe little difference in scaling for $X^{(3,4)}$ and $X^{(2,3)}X^{(4,5)}$, but $X^{(2,5)}$ – with its larger distance between states – appears to converge more slowly for $S + D$. Notice how $\mathcal{I}$ is not strongly affected by applying multiple $X$-gates – confirming the S+D observation and suggesting it also holds for ECD decompositions. For the $R_X^{(3,4)}(\theta)$ gates, $\mathcal{I}$ increases with $\theta$ for both decompositions. Further, for fixed $B$, For the small $\theta$ investigated here, $R_X$ has lower $\mathcal{I}$ that $X$ gates. In all cases $B_{S+D} \ll B_{ECD}$ with the relative factor being $\sim 6 = d$ which comports with the scaling from parameter counting.

After looking at the dependence of $\mathcal{I}$ on the two decomposition methods, we perform an analysis of two gates $X^{(3,4)}$ and $R_X^{(3,4)}(\pi/10)$ for $d = 4, 6, 8$ qudits which is presented in Fig. (10). If we take as a fiducial $\mathcal{I} = 10^{-4}$, we find that nearly constant $B_{S+D} \sim 2-3$ for all $d$, while $B_{ECD} = 16, 36, 64$ for $d = 4, 6, 8$ respectively. This again suggests $B_{S+D}$ scales sublinearly with $d$. In contrast, ECD scales consistently with $B_{ECD} \sim d^2$.

Taking these results, one can estimate the break-even dimension $d_b$ when the decompositions require the same amount of time by setting

$$B_{ECD}T_{ECD} = B_{S+D}T_{S+D}. \tag{35}$$

TABLE II. $\mathcal{I}_{PO}$ of two gates obtained with pulse optimization for qudits. For all cases, the time interval was divided into 50 time steps and the best optimization of 10 trials was taken. The final truncation order of the Chebysev series is denoted by $o_C$.

| d | T [$\mu$s] | $o_C$ | $X$ | $R_x$ |
|---|---|---|---|---|
| 4 | 0.5 | 18 | $4 \times 10^{-5}$ | $5 \times 10^{-7}$ |
| 6 | 0.5 | 30 | $3 \times 10^{-5}$ | $6 \times 10^{-5}$ |
| 8 | 2.0 | 50 | $2 \times 10^{-3}$ | $2 \times 10^{-3}$ |

With the empirically-observed constant $B_{S+D}$ and relative factor of $\sim 1$ between the decompositions, one finds

$$\frac{T_{S+D}}{T_{ECD}} = d_b^2 \implies d_b = \sqrt{\frac{[1, 50] \ \mu s}{[0.1, 0.5] \ \mu s}} = [2, 22], \tag{36}$$

if instead, one takes the scaling suggested from parameter counting $B_{S+D} = d$, the range is $d_b = [2, 500]$. These heuristics suggest while neither gate decomposition is decisively better, hardware-obtainable $T_{S+D}$ and $T_{ECD}$ would resolve it.

This logic can also be used to estimate the number of HEP primitive gates could be simulated within $T_1 = 10$ ms of the qudit with fixed $\mathcal{I}$ versus $B$. In Fig. 11 is a fiducial result for the $R_X^{(3,4)}(\pi/10)$ gate decomposition on a quoctit with fixed gate times of $T_{S+D} = 1 \ \mu s$ and $T_{ECD} = 0.2 \ \mu s$. Together these suggest such devices could reasonably achieve circuit depth of thousands of gates with total $\mathcal{I} < 1\%$. Given the resources estimates for $SU(2)$ in [49], this would be sufficient for quantum utility in toy models.

Finally, we consider optimal control. The pulse duration $T_{PO} = 0.5 \ \mu s$ for the ququart and quhexit to be competitive with the single-block gate set decompositions, but had to be extended to 2 $\mu s$ for the quoctit to get $\mathcal{I} < 10^{-2}$. An example of the resulting pulses is shown in Fig. (12). The lowest infidelity from 10 trials for all three qudit dimensions are shown in Table II. An additional optimization that proved useful for the quoctit was to start with a smaller basis set, truncated at the 32th order. Then every 500 iterations, new terms were added to the decomposition. The new terms were added in 3 different batches consisting of 8, 5 and 5.

For the case of the quhexit, the infidelity from pulse optimization $\mathcal{I}_{PO} \lesssim 10^{-5}$ was close to that of a 5-block $\mathcal{I}_{S+D}$ and a 36 block $\mathcal{I}_{ECD}$ which allows us to make a direct comparison in this case of the relative gate time for the $X^{(3,4)}$ and $R_X^{(3,4)}(\pi/10)$:

$$T_{PO}^6 \approx 0.5 \ \mu s$$
$$T_{S+D}^6 \approx [5, 250] \ \mu s$$
$$T_{ECD}^6 \approx [3.6, 18] \ \mu s.$$

Thus we find that pulse optimization for $X^{(3,4)}$ and $R_X^{(3,4)}(\pi/10)$ at fixed infidelity appears to yield at least
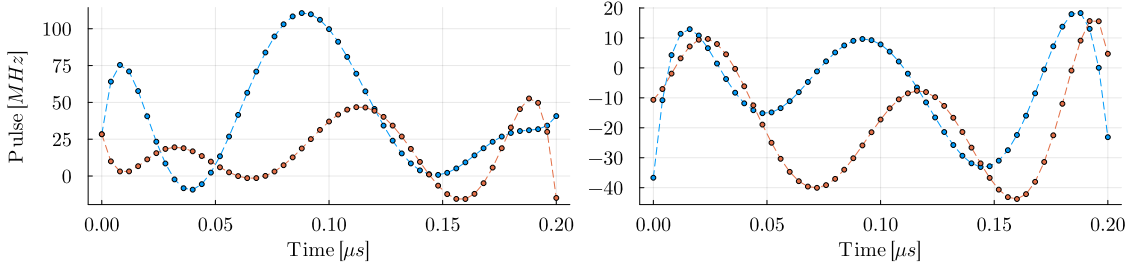
FIG. 8. Pulse optimization for the state prep of $H_6 |0\rangle = \frac{1}{\sqrt{6}} \sum_i |i\rangle$ for a quhexit
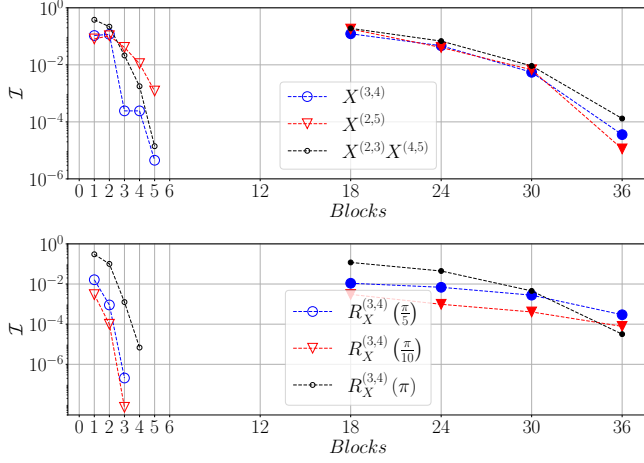


FIG. 9. $\mathcal{I}$ vs. blocks for S+D and ECD for quhexit gates.

a factor of 10 in reduction of gate time. For the quoctit, we can similarly compare to the gate sets, albeit only at a higher $\mathcal{I} \lesssim 10^{-3}$ since that was the best obtained from pulse optimization. For comparable infidelities a 4-block $S + D$ and 64-block ECD were found sufficient,

$$T_{PO}^8 \approx 2.0 \ \mu s$$
$$T_{S+D}^8 \approx [4, 200] \ \mu s$$
$$T_{\mathrm{ECD}}^8 \approx [6.4, 32] \ \mu s.$$

In this case, the improvement was a more modest factor for 2, which may indicate a diminishing in advantage at higher dimension or a reflection of the difficulty of classical optimization at high dimension.

While these results demonstrate it is possible to decompose gates of interest to a universal set, the decomposition generically has poor scaling $\mathcal{O}(d^n)$ with $n \geq 3$ [150, 154, 164] that without mitigation will become prohibitive for large $d$. It is therefore worth investigating the relations between optimized parameters to seek heuristics to guide the optimization. Since $S + D$ requires fewer blocks than ECD, we will restrict our analysis to this decomposition and study the 5-block versions of $X^{(3,4)}$, $X^{(2,3)} X^{(4,5)}$, $R_X^{(3,4)}(\pi/10)$ gates acting on a quhexit. The optimization is performed 200 times for each gate. The distributions of $\mathcal{I}$ are shown in Fig. (13), where one ob-
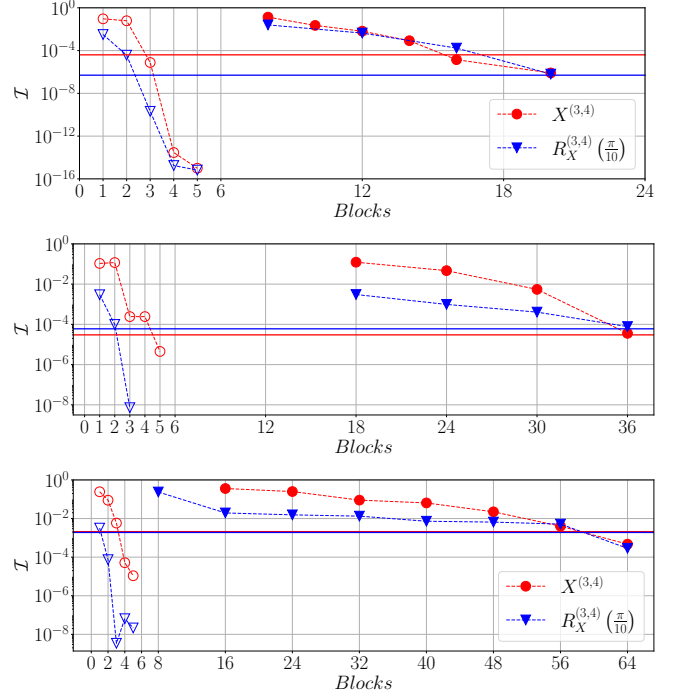


FIG. 10. $\mathcal{I}$ vs blocks for $S + D$ and ECD decomposition of an $X^{(3,4)}$ and $R_x^{(3,4)}(\pi/10)$ gate, for ququart, quhexit and quoctit from top to bottom. The horizontal lines correspond to the reference values of the PO infidelities.
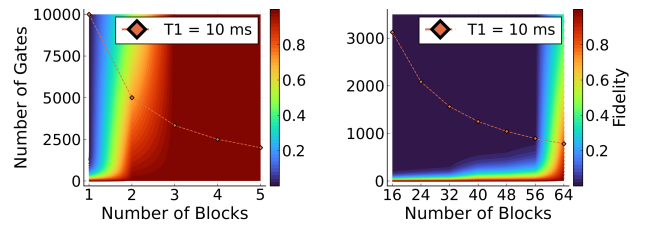


FIG. 11. $R_X^{(3,4)}(\pi/10)$ gate decomposition on quoctit using (left) $S + D$ and (right) ECD. The $T_1$ is plotted as a reference for the maximum number of gates given a certain amount of blocks, assuming fixed gate times of $T_{SNAP} = 1\mu s$ and $T_{ECD} = 200ns$.
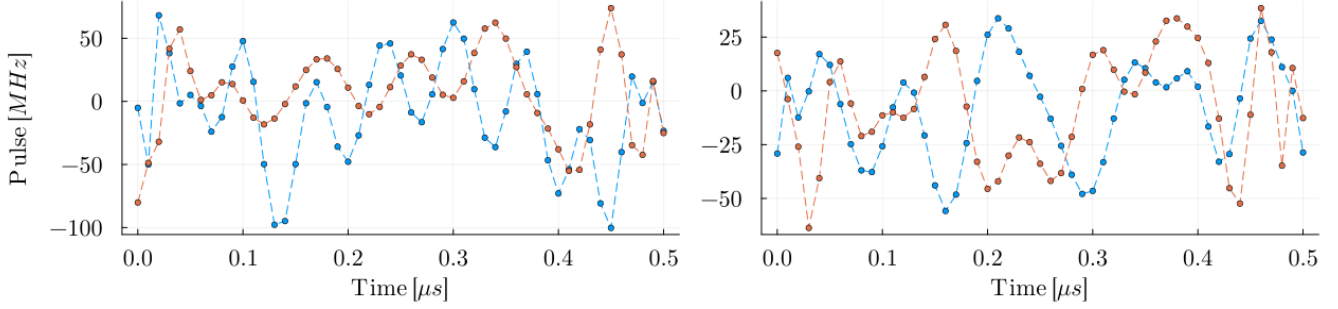
FIG. 12. Example $X$ gate pulses for a quhexit, with a control on the pulses every $10ns$.
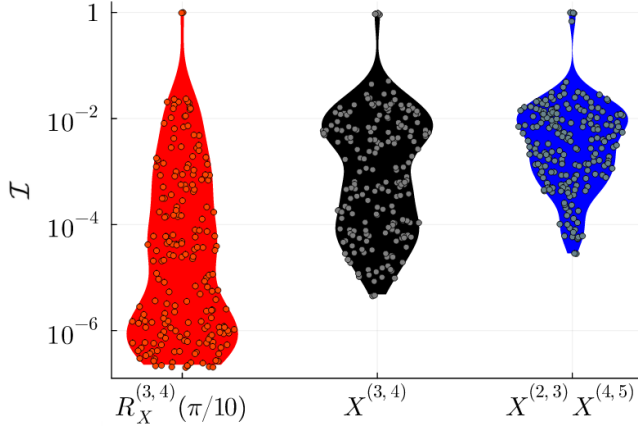


FIG. 13. Distribution of infidelities for 5-block $S + D$ decomposition for different quhexit gates starting from the same initial parameters.
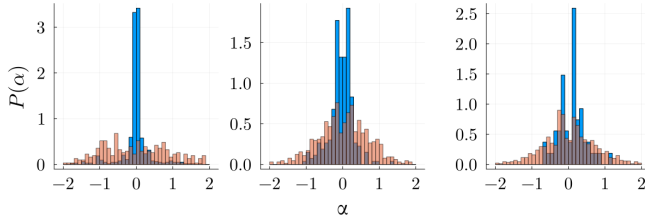


FIG. 14. Distribution of $\alpha_k$ of quhexit optimizations that gave $\mathcal{I} > 10^{-4}$ (orange) and $\mathcal{I} \leq 10^{-4}$ (blue). From left to right for $R_X^{(3,4)}(\pi/10)$, $X^{(3,4)}$ and $X^{(2,3)}X^{(4,5)}$

serves a clear ordering of $\mathcal{I}$ from smallest to largest of $R_X^{(3,4)}(\pi/10)$, $X^{(3,4)}$, $X^{(2,3)}X^{(4,5)}$. This supports the intuition that the distance from $\mathbb{1}$ is a proxy for difficulty.

Probing further, one can study the distribution of $S+D$ parameters. The distribution of the SNAP $\theta_k$ appear to be uniformly distributed regardless of $\mathcal{I}$. In contrast, the displacement parameters clearly distinguish between good and poor optimizations as seen in Fig. (14). For $\mathcal{I} \leq 10^{-4}$ where $\alpha$ cluster near 0, compared to optimizations where $\mathcal{I} \geq 10^{-4}$ that have broader distributions. This can be used to reduce the search parameter space.
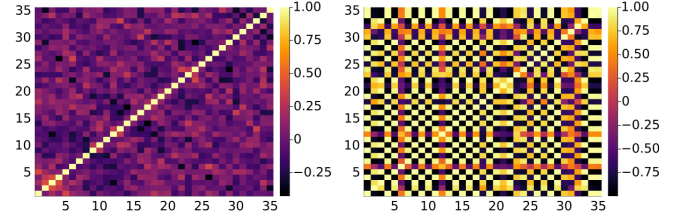


FIG. 15. Correlation matrix across parameters for $S + D$ decompositions of $X^{(3,4)}$ gate for a 5-block quhexit optimizations with (left) $\mathcal{I} \leq 10^{-5}$ and (right) $\mathcal{I} > 10^{-5}$.

Another source for accelerating the optimization would use correlations between the optimal parameters. This is further motivated by empirical observations that for optimal $B_{S+D} = 1$ decompositions $\alpha_1 = -\alpha_0$ of many gates. We searched for correlations across optimizations of $X^{(3,4)}$. Fig. (15) shows the correlation matrix corresponding to high and low infidelities. The correlation between two decomposition parameters $X, Y \in \{\alpha_k, \theta_k\}$ were computed using

$$\rho(X, Y) = \frac{1}{\sigma_X \sigma_Y (n-1)} \sum_{i=1}^{n} (X_i - \bar{X})(Y_i - \bar{Y}),$$

where $\sigma_X$ and $\bar{X}$ are the standard deviation and mean of $X$. From the analysis of these correlations, we found different distributions when comparing low and high infidelity decompositions, when $\mathcal{I} > 10^{-5}$ the parameters are highly symmetric and with large correlation (or anticorrelation). In contrast, for $\mathcal{I} \leq 10^{-5}$ the parameters display decreasing correlation with gates farther away in the decomposition i.e. gates in the same block are more correlated. Additionally, there is some clear, weak anti-correlation structure suggesting new ansatze for decomposition. Moreover, we found that the same initial conditions gave either good results for two different gates, or bad results for both. This is presented in Fig. 16 and suggests that there might be only a subspace of the parameters. However, this hypothesis requires more analytical work should be explored in the future.

A final consideration is the robustness to quantum noise. As a first step toward understand this, we studied how
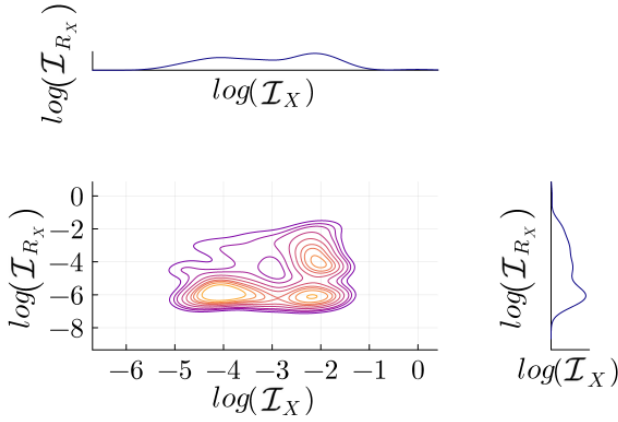
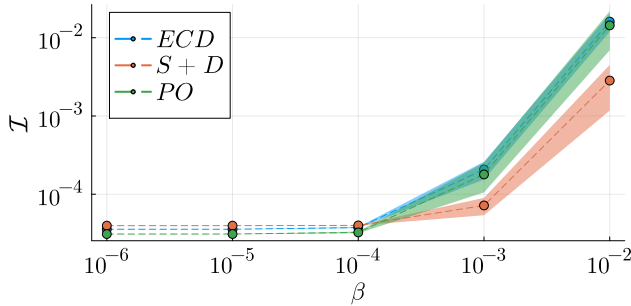FIG. 16. Contours of the infidelities reached from same initial parameters for a $R_X$ and a $X$ gate.



FIG. 17. Stability analysis for all the decompositions for a $X$ gate on a quhexit.

$\mathcal{I}$ degrades when the parameters of the gate sets and pulse optimization were perturbed by a Gaussian noise. This basic noise model could be taken to approximate the stochastic fluctuations in the pulses driving the cavity and qubit. In this model the parameters are varied:

$$\alpha \to \alpha(x) = \alpha + \frac{1}{\beta|\alpha|\sqrt{2\pi}} \exp^{-\frac{1}{2}\left(\frac{x}{\beta|\alpha|}\right)^2}, \qquad (37)$$

where $\alpha$ is the parameter of the decomposition, and $\beta$ is the square-root of the variance.

Taking the noiseless $X^{(3,4)}$ gates on the quhexit with $\mathcal{I} \approx 10^{-5}$: 5-block $S + D$ with $\mathcal{I} = 3.97 \times 10^{-5}$, 36-block ECD with $\mathcal{I} = 3.57 \times 10^{-5}$, and 30th order pulse optimization for 0.5 $\mu$s with $\mathcal{I} = 3.10 \times 10^{-5}$; 50 random sample perturbations for each $\beta$ are computed. The plot showing the results is Fig. (17). One observes that for $\beta < 10^{-4}$, the effect of noise is negligible. At larger $\beta$, pulse optimization and $ECD$ are found to demonstrate similar sized infidelities from the noise, while $S + D$ is found to have $\mathcal{I}$ about half the size of the other two.

## VII. CONCLUSION

In this work, we compared the three methods for implementing prototypical primitive gates for simulating lattice gauge theories on a 3D SRF qudit architecture: Snap & Displacement gates, ECD & single-qubit rotations, and optimal pulse control. We observed that lattice gauge theory primitives have common properties that distinguish them from general $SU(d)$ circuits, and thus the choice of decomposition could greatly change the algorithmic reach of devices. We found evidence that for subsets of permutation gates the number of SNAP and Displacement blocks required to approximate them scales sublinearly with qudit dimension – in contrast to the general case of linear scaling –, while the ECD block depth quadratically. In all cases, we found that decomposing a sequence of $X^{(a,b)}$ gates rather than individual reduces the total number of blocks required and consequently the total time for fixed infidelity. With the gate sets, we found that $\mathcal{I} < 10^{-5}$ is possible for $B_{S+D} = d$ and $B_{ECD} = d^2$. In addition, pulse decomposition with modest classical resources can outperform in run time for $d < 8$, while becoming comparable to gate decomposition for quoctits. Beyond run time, the $S + D$ decomposition was found to be more robust to Gaussian perturbations.

From the analysis of the $S+D$ decomposition, we found that good gate decompositions can be distinguished by symmetries, correlations, and the distribution of parameters. Further, we found correlations between initial conditions, suggesting a subspace useful as initial conditions.

From this initial work, we found that algorithmic advantage and hardware-specific gate times can be used to decisively choose between different native gate sets on qudit devices for the restricted class of gates needed for high energy physics. In the future, more in-depth investigation of the scaling of the decompositions should be performed. Further, it would be of invaluable help to try to implement some of the decompositions on the actual hardware, in order to better understand and develop a noise model and how the infidelities are affected.

[1] N. Klco, A. Roggero, and M. J. Savage, Standard model physics and the digital quantum revolution: thoughts about the interface, Rept. Prog. Phys. **85**, 064301 (2022),

arXiv:2107.04769 [quant-ph].

[2] M. C. Bañuls *et al.*, Simulating Lattice Gauge Theories within Quantum Technologies, Eur. Phys. J. D **74**, 165 (2020), arXiv:1911.00003 [quant-ph].

[3] C. W. Bauer *et al.*, Quantum Simulation for High-Energy Physics, PRX Quantum **4**, 027001 (2023), arXiv:2204.03381 [quant-ph].

[4] A. Di Meglio *et al.*, Quantum Computing for High-Energy Physics: State of the Art and Challenges. Summary of the QC4HEP Working Group (2023), arXiv:2307.03236 [quant-ph].

[5] E. J. Gustafson, Y. Ji, H. Lamm, E. M. Murairi, S. O. Perez, and S. Zhu, Primitive quantum gates for an SU(3) discrete subgroup: $\Sigma(36\times3)$, Phys. Rev. D **110**, 034515 (2024), arXiv:2405.05973 [hep-lat].

[6] M. Rhodes, M. Kreshchuk, and S. Pathak, Exponential improvements in the simulation of lattice gauge theories using near-optimal techniques (2024), arXiv:2405.10416 [quant-ph].

[7] E. Gustafson *et al.*, Large scale multi-node simulations of $\mathbb{Z}_2$ gauge theory quantum circuits using Google Cloud Platform, in *IEEE/ACM Second International Workshop on Quantum Computing Software* (2021) arXiv:2110.07482 [quant-ph].

[8] E. Gustafson, Prospects for Simulating a Qudit Based Model of (1+1)d Scalar QED, Phys. Rev. D **103**, 114505 (2021), arXiv:2104.10136 [quant-ph].

[9] P. P. Popov, M. Meth, M. Lewenstein, P. Hauke, M. Ringbauer, E. Zohar, and V. Kasper, Variational quantum simulation of U(1) lattice gauge theories with qudit systems, Phys. Rev. Res. **6**, 013202 (2024).

[10] D. M. Kurkcuoglu, M. S. Alam, J. A. Job, A. C. Y. Li, A. Macridin, G. N. Perdue, and S. Providence, Quantum simulation of $\phi^4$ theories in qudit systems (2021), arXiv:2108.13357 [quant-ph].

[11] G. Calajò, G. Magnifico, C. Edmunds, M. Ringbauer, S. Montangero, and P. Silvi, Digital quantum simulation of a (1+1)D SU(2) lattice gauge theory with ion qudits (2024), arXiv:2402.07987 [quant-ph].

[12] D. González-Cuadra, T. V. Zache, J. Carrasco, B. Kraus, and P. Zoller, Hardware efficient quantum simulation of non-abelian gauge theories with qudits on Rydberg platforms (2022), arXiv:2203.15541 [quant-ph].

[13] M. Illa, C. E. P. Robin, and M. J. Savage, Qu8its for quantum simulations of lattice quantum chromodynamics, Phys. Rev. D **110**, 014507 (2024), arXiv:2403.14537 [quant-ph].

[14] T. V. Zache, D. González-Cuadra, and P. Zoller, Fermion-qudit quantum processors for simulating lattice gauge theories with matter, Quantum **7**, 1140 (2023), arXiv:2303.08683 [quant-ph].

[15] D. Janković, J.-G. Hartmann, M. Ruben, and P.-A. Hervieux, Noisy qudit vs multiple qubits: conditions on gate efficiency for enhancing fidelity, npj Quantum Information **10**, 59 (2024).

[16] A. S. Nikolaeva, E. O. Kiktenko, and A. K. Fedorov, Efficient realization of quantum algorithms with qudits, EPJ Quant. Technol. **11**, 43 (2024), arXiv:2111.04384 [quant-ph].

[17] M. B. Mansky, S. L. n. Castillo, V. R. Puigvert, and C. Linnhoff-Popien, Near-optimal quantum circuit construction via Cartan decomposition, Phys. Rev. A **108**, 052607 (2023), arXiv:2212.12934 [quant-ph].

[18] M. Ringbauer, M. Meth, L. Postler, R. Stricker, R. Blatt, P. Schindler, and T. Monz, A universal qudit quantum processor with trapped ions, Nature Phys. **18**, 1053 (2022), arXiv:2109.06903 [quant-ph].

[19] A. S. Nikolaeva *et al.*, Scalable improvement of the generalized Toffoli gate realization using trapped-ion-based qutrits (2024), arXiv:2407.07758 [quant-ph].

[20] P. J. Low, B. White, and C. Senko, Control and Readout of a 13-level Trapped Ion Qudit (2023), arXiv:2306.03340 [quant-ph].

[21] N. Goss *et al.*, High-fidelity qutrit entangling gates for superconducting circuits, Nature Commun. **13**, 7481 (2022), [Erratum: Nature Commun. 14, 4256 (2023)], arXiv:2206.07216 [quant-ph].

[22] K. Luo *et al.*, Experimental Realization of Two Qutrits Gate with Tunable Coupling in Superconducting Circuits, Phys. Rev. Lett. **130**, 030603 (2023), arXiv:2206.11199 [quant-ph].

[23] N. Goss, S. Ferracin, A. Hashim, A. Carignan-Dugas, J. M. Kreikebaum, R. K. Naik, D. I. Santiago, and I. Siddiqi, Extending the Computational Reach of a Superconducting Qutrit Processor (2023), arXiv:2305.16507 [quant-ph].

[24] S. Cao, M. Bakr, G. Campanaro, S. D. Fasciati, J. Wills, D. Lall, B. Shteynas, V. Chidambaram, I. Rungger, and P. Leek, Emulating two qubits with a four-level transmon qudit for variational quantum algorithms, Quantum Sci. Technol. **9**, 035003 (2024), arXiv:2303.04796 [quant-ph].

[25] L. M. Seifert, Z. Li, T. Roy, D. I. Schuster, F. T. Chong, and J. M. Baker, Exploring ququart computation on a transmon using optimal control, Phys. Rev. A **108**, 062609 (2023), arXiv:2304.11159 [quant-ph].

[26] Z. Wang, R. W. Parker, E. Champion, and M. S. Blok, Systematic study of High $E_J/E_C$ transmon qudits up to $d = 12$ (2024), arXiv:2407.17407 [quant-ph].

[27] A. Kruckenhauser, R. van Bijnen, T. V. Zache, M. Di Liberto, and P. Zoller, High-dimensional SO(4)-symmetric Rydberg manifolds for quantum simulation, Quantum Sci. Technol. **8**, 015020 (2023), arXiv:2206.01108 [quant-ph].

[28] S. R. Cohen and J. D. Thompson, Quantum Computing with Circular Rydberg Atoms, PRX Quantum **2**, 030322 (2021).

[29] Y. Chi *et al.*, A programmable qudit-based quantum processor, Nature Commun. **13**, 1166 (2022).

[30] V. Kasper, D. González-Cuadra, A. Hegde, A. Xia, A. Dauphin, F. Huber, E. Tiemann, M. Lewenstein, F. Jendrzejewski, and P. Hauke, Universal quantum computation and quantum error correction with ultracold atomic mixtures, Quantum Sci. Technol. **7**, 015008 (2022), arXiv:2010.15923 [cond-mat.quant-gas].

[31] T. Roy, T. Kim, A. Romanenko, and A. Grassellino, Qudit-based quantum computing with SRF cavities at Fermilab, PoS **LATTICE2023**, 127 (2024).

[32] R. W. Heeres, B. Vlastakis, E. Holland, S. Krastanov, V. V. Albert, L. Frunzio, L. Jiang, and R. J. Schoelkopf, Cavity state manipulation using photon-number selective phase gates, Physical Review Letters **115**, 10.1103/physrevlett.115.137002 (2015).

[33] T. Fösel, S. Krastanov, F. Marquardt, and L. Jiang, Efficient cavity control with SNAP gates (2020), arXiv:2004.14256 [quant-ph].

[34] M. Kudra, M. Kervinen, I. Strandberg, S. Ahmed, M. Scigliuzzo, A. Osman, D. P. Lozano, M. O. Tholén, R. Borgani, D. B. Haviland, G. Ferrini, J. Bylander, A. F.

Kockum, F. Quijandría, P. Delsing, and S. Gasparinetti, Robust preparation of wigner-negative states with optimized SNAP-displacement sequences, PRX Quantum **3**, 10.1103/prxquantum.3.030301 (2022).

[35] A. Eickbusch, V. Sivak, A. Z. Ding, S. S. Elder, S. R. Jha, J. Venkatraman, B. Royer, S. M. Girvin, R. J. Schoelkopf, and M. H. Devoret, Fast universal control of an oscillator with weak dispersive coupling to a qubit, Nature Phys. **18**, 1464 (2022), arXiv:2111.06414 [quant-ph].

[36] G. K. Brennen, S. S. Bullock, and D. P. O'Leary, Efficient circuits for exact-universal computation with qudits, Quant. Inf. Comput. **6**, 436 (2006).

[37] M. Howard and J. Vala, Qudit versions of the qubit $\pi/8$ gate, Phys. Rev. A **86**, 022316 (2012).

[38] A. Bocharov, A note on optimality of quantum circuits over metaplectic basis, Quant. Inf. Comput. **18**, 0001 (2018).

[39] L. Yeh and J. van de Wetering, Constructing all qutrit controlled Clifford+T gates in Clifford+T., Lect. Notes Comput. Sci. **13354**, 28 (2022), arXiv:2204.00552 [quant-ph].

[40] Y. Nakajima, Y. Kawano, H. Sekigawa, M. Nakanishi, S. Yamashita, and Y. Nakashima, Synthesis of quantum circuits for $d$-level systems by using cosine-sine, Quant. Inf. Comput. **9**, 0423 (2009).

[41] S. Prakash, A. R. Kalra, and A. Jain, A normal form for single-qudit Clifford+T operators, Quant. Inf. Proc. **20**, 341 (2021).

[42] A. R. Kalra, D. Valluri, and M. Mosca, Synthesis and Arithmetic of Single Qutrit Circuits (2023), arXiv:2311.08696 [quant-ph].

[43] R. I. Booth and T. Carette, Complete ZX-calculi for the stabiliser fragment in odd prime dimensions (2022), arXiv:2204.12531 [quant-ph].

[44] A. N. Glaudell, N. J. Ross, J. van de Wetering, and L. Yeh, Qutrit Metaplectic Gates Are a Subset of Clifford+T, Leibniz Int. Proc. Inf. **232**, 12:1 (2022), arXiv:2202.09235 [quant-ph].

[45] A. N. Glaudell, N. J. Ross, J. van de Wetering, and L. Yeh, Exact Synthesis of Multiqutrit Clifford-Cyclotomic Circuits, EPTCS **406**, 44 (2024), arXiv:2405.08136 [quant-ph].

[46] S. Prakash, A. Jain, B. Kapur, and S. Seth, Normal form for single-qutrit Clifford+$T$ operators and synthesis of single-qutrit gates, Phys. Rev. A **98**, 032304 (2018), arXiv:1803.03228 [quant-ph].

[47] H. Lamm, S. Lawrence, and Y. Yamauchi (NuQS), General Methods for Digital Quantum Simulation of Gauge Theories, Phys. Rev. **D100**, 034518 (2019), arXiv:1903.08807 [hep-lat].

[48] M. S. Alam, S. Hadfield, H. Lamm, and A. C. Y. Li (SQMS), Primitive quantum gates for dihedral gauge theories, Phys. Rev. D **105**, 114501 (2022), arXiv:2108.13305 [quant-ph].

[49] E. J. Gustafson, H. Lamm, F. Lovelace, and D. Musk, Primitive quantum gates for an SU(2) discrete subgroup: Binary tetrahedral, Phys. Rev. D **106**, 114501 (2022), arXiv:2208.12309 [quant-ph].

[50] T. V. Zache, D. González-Cuadra, and P. Zoller, Quantum and Classical Spin-Network Algorithms for q-Deformed Kogut-Susskind Gauge Theories, Phys. Rev. Lett. **131**, 171902 (2023), arXiv:2304.02527 [quant-ph].

[51] E. J. Gustafson, H. Lamm, and F. Lovelace, Primitive quantum gates for an SU(2) discrete subgroup: Binary octahedral, Phys. Rev. D **109**, 054503 (2024), arXiv:2312.10285 [hep-lat].

[52] H. Lamm, Y.-Y. Li, J. Shu, Y.-L. Wang, and B. Xu, Block Encodings of Discrete Subgroups on Quantum Computer (2024), arXiv:2405.12890 [hep-lat].

[53] E. M. Murairi, M. Sohaib Alam, H. Lamm, S. Hadfield, and E. Gustafson, Highly-efficient quantum Fourier transformations for some nonabelian groups (2024), arXiv:2408.00075 [quant-ph].

[54] T. D. Cohen, H. Lamm, S. Lawrence, and Y. Yamauchi (NuQS), Quantum algorithms for transport coefficients in gauge theories, Phys. Rev. D **104**, 094514 (2021), arXiv:2104.02024 [hep-lat].

[55] M. Carena, H. Lamm, Y.-Y. Li, and W. Liu, Improved Hamiltonians for Quantum Simulations of Gauge Theories, Phys. Rev. Lett. **129**, 051601 (2022), arXiv:2203.02823 [hep-lat].

[56] E. J. Gustafson, Stout Smearing on a Quantum Computer (2022), arXiv:2211.05607 [hep-lat].

[57] E. Gustafson and R. Van de Water, Improved Fermion Hamiltonians for Quantum Simulation, PoS **LATTICE2023**, 215 (2024), arXiv:2402.04317 [hep-lat].

[58] M. Carena, H. Lamm, Y.-Y. Li, and W. Liu, Quantum error thresholds for gauge-redundant digitizations of lattice field theories (2024), arXiv:2402.16780 [hep-lat].

[59] E. Zohar, J. I. Cirac, and B. Reznik, Cold-Atom Quantum Simulator for SU(2) Yang-Mills Lattice Gauge Theory, Phys. Rev. Lett. **110**, 125304 (2013), arXiv:1211.2241 [quant-ph].

[60] E. Zohar, J. I. Cirac, and B. Reznik, Simulating Compact Quantum Electrodynamics with ultracold atoms: Probing confinement and nonperturbative effects, Phys. Rev. Lett. **109**, 125302 (2012), arXiv:1204.6574 [quant-ph].

[61] E. Zohar, J. I. Cirac, and B. Reznik, Quantum simulations of gauge theories with ultracold atoms: local gauge invariance from angular momentum conservation, Phys. Rev. **A88**, 023617 (2013), arXiv:1303.5040 [quant-ph].

[62] E. Zohar, J. I. Cirac, and B. Reznik, Quantum Simulations of Lattice Gauge Theories using Ultracold Atoms in Optical Lattices, Rept. Prog. Phys. **79**, 014401 (2016), arXiv:1503.02312 [quant-ph].

[63] A. Bazavov, Y. Meurice, S.-W. Tsai, J. Unmuth-Yockey, and J. Zhang, Gauge-invariant implementation of the Abelian Higgs model on optical lattices, Phys. Rev. **D92**, 076003 (2015), arXiv:1503.08354 [hep-lat].

[64] J. Zhang, J. Unmuth-Yockey, J. Zeiher, A. Bazavov, S. W. Tsai, and Y. Meurice, Quantum simulation of the universal features of the Polyakov loop, Phys. Rev. Lett. **121**, 223201 (2018), arXiv:1803.11166 [hep-lat].

[65] J. Unmuth-Yockey, J. Zhang, A. Bazavov, Y. Meurice, and S.-W. Tsai, Universal features of the Abelian Polyakov loop in 1+1 dimensions, Phys. Rev. **D98**, 094511 (2018), arXiv:1807.09186 [hep-lat].

[66] N. Klco, J. R. Stryker, and M. J. Savage, SU(2) non-Abelian gauge field theory in one dimension on digital quantum computers, Phys. Rev. D **101**, 074512 (2020), arXiv:1908.06935 [quant-ph].

[67] R. C. Farrell, M. Illa, A. N. Ciavarella, and M. J. Savage, Scalable Circuits for Preparing Ground States on Digital Quantum Computers: The Schwinger Model Vacuum on 100 Qubits (2023), arXiv:2308.04481 [quant-ph].

[68] R. C. Farrell, M. Illa, A. N. Ciavarella, and M. J. Savage, Quantum Simulations of Hadron Dynamics in the Schwinger Model using 112 Qubits (2024),

arXiv:2401.08044 [quant-ph].

[69] A. Ciavarella, N. Klco, and M. J. Savage, A Trailhead for Quantum Simulation of SU(3) Yang-Mills Lattice Gauge Theory in the Local Multiplet Basis (2021), arXiv:2101.10227 [quant-ph].

[70] A. Bazavov, S. Catterall, R. G. Jha, and J. Unmuth-Yockey, Tensor renormalization group study of the non-abelian higgs model in two dimensions, Phys. Rev. D **99**, 114507 (2019).

[71] A. J. Buser, T. Bhattacharya, L. Cincio, and R. Gupta, Quantum simulation of the qubit-regularized O(3)-sigma model (2020), arXiv:2006.15746 [quant-ph].

[72] T. Bhattacharya, A. J. Buser, S. Chandrasekharan, R. Gupta, and H. Singh, Qubit regularization of asymptotic freedom (2020), arXiv:2012.02153 [hep-lat].

[73] A. H. Z. Kavaki and R. Lewis, From square plaquettes to triamond lattices for SU(2) gauge theory (2024), arXiv:2401.14570 [hep-lat].

[74] E. M. Murairi, M. J. Cervia, H. Kumar, P. F. Bedaque, and A. Alexandru, How many quantum gates do gauge theories require? (2022), arXiv:2208.11789 [hep-lat].

[75] Z. Davoudi, C.-C. Hsieh, and S. V. Kadam, Scattering wave packets of hadrons in gauge theories: Preparation on a quantum computer (2024), arXiv:2402.00840 [quant-ph].

[76] I. Raychowdhury and J. R. Stryker, Solving Gauss's Law on Digital Quantum Computers with Loop-String-Hadron Digitization (2018), arXiv:1812.07554 [hep-lat].

[77] S. V. Kadam, *Theoretical Developments in Lattice Gauge Theory for Applications in Double-beta Decay Processes and Quantum Simulation*, Ph.D. thesis, Maryland U., College Park (2023), arXiv:2312.00780 [hep-lat].

[78] Z. Davoudi, I. Raychowdhury, and A. Shaw, Search for Efficient Formulations for Hamiltonian Simulation of non-Abelian Lattice Gauge Theories (2020), arXiv:2009.11802 [hep-lat].

[79] E. Mathew and I. Raychowdhury, Protecting local and global symmetries in simulating (1+1)D non-Abelian gauge theories, Phys. Rev. D **106**, 054510 (2022), arXiv:2206.07444 [hep-lat].

[80] C. W. Bauer and D. M. Grabowska, Efficient Representation for Simulating U(1) Gauge Theories on Digital Quantum Computers at All Values of the Coupling (2021), arXiv:2111.08015 [hep-ph].

[81] D. M. Grabowska, C. Kane, B. Nachman, and C. W. Bauer, Overcoming exponential scaling with system size in Trotter-Suzuki implementations of constrained Hamiltonians: 2+1 U(1) lattice gauge theories (2022), arXiv:2208.03333 [quant-ph].

[82] D. M. Grabowska, C. F. Kane, and C. W. Bauer, A Fully Gauge-Fixed SU(2) Hamiltonian for Quantum Simulations (2024), arXiv:2409.10610 [quant-ph].

[83] T. Li, Quantum simulations of quantum electrodynamics in Coulomb gauge (2024), arXiv:2406.01204 [hep-lat].

[84] M. Kreshchuk, W. M. Kirby, G. Goldstein, H. Beauchemin, and P. J. Love, Quantum Simulation of Quantum Field Theory in the Light-Front Formulation (2020), arXiv:2002.04016 [quant-ph].

[85] M. Kreshchuk, S. Jia, W. M. Kirby, G. Goldstein, J. P. Vary, and P. J. Love, Simulating Hadronic Physics on NISQ devices using Basis Light-Front Quantization (2020), arXiv:2011.13443 [quant-ph].

[86] M. Kreshchuk, S. Jia, W. M. Kirby, G. Goldstein, J. P. Vary, and P. J. Love, Light-Front Field Theory on Current Quantum Computers (2020), arXiv:2009.07885 [quant-ph].

[87] J. Liu and Y. Xin, Quantum simulation of quantum field theories as quantum chemistry (2020), arXiv:2004.13234 [hep-th].

[88] M. Fromm, O. Philipsen, W. Unger, and C. Winterowd, Quantum Gate Sets for Lattice QCD in the strong coupling limit: $N_f = 1$ (2023), arXiv:2308.03196 [hep-lat].

[89] A. N. Ciavarella and C. W. Bauer, Quantum Simulation of SU(3) Lattice Yang Mills Theory at Leading Order in Large N (2024), arXiv:2402.10265 [hep-ph].

[90] A. Alexandru, P. F. Bedaque, A. Carosso, M. J. Cervia, E. M. Murairi, and A. Sheng, Fuzzy gauge theory for quantum computers, Phys. Rev. D **109**, 094502 (2024), arXiv:2308.05253 [hep-lat].

[91] R. Brower, S. Chandrasekharan, and U. J. Wiese, QCD as a quantum link model, Phys. Rev. **D60**, 094502 (1999), arXiv:hep-th/9704106 [hep-th].

[92] H. Singh, Qubit $O(N)$ nonlinear sigma models (2019), arXiv:1911.12353 [hep-lat].

[93] H. Singh and S. Chandrasekharan, Qubit regularization of the $O(3)$ sigma model, Phys. Rev. D **100**, 054505 (2019), arXiv:1905.13204 [hep-lat].

[94] U.-J. Wiese, Towards Quantum Simulating QCD, *Proceedings, 24th International Conference on Ultra-Relativistic Nucleus-Nucleus Collisions (Quark Matter 2014): Darmstadt, Germany, May 19-24, 2014*, Nucl. Phys. **A931**, 246 (2014), arXiv:1409.7414 [hep-th].

[95] R. C. Brower, D. Berenstein, and H. Kawai, Lattice Gauge Theory for a Quantum Computer, PoS **LATTICE2019**, 112 (2019), arXiv:2002.10028 [hep-lat].

[96] S. V. Mathis, G. Mazzola, and I. Tavernelli, Toward scalable simulations of Lattice Gauge Theories on quantum computers, Phys. Rev. D **102**, 094501 (2020), arXiv:2005.10271 [quant-ph].

[97] J. C. Halimeh, R. Ott, I. P. McCulloch, B. Yang, and P. Hauke, Robustness of gauge-invariant dynamics against defects in ultracold-atom gauge theories, Phys. Rev. Res. **2**, 033361 (2020), arXiv:2005.10249 [cond-mat.quant-gas].

[98] T. Budde, M. K. Marinković, and J. C. P. Barros, Quantum many-body scars for arbitrary integer spin in $2 + 1$d abelian gauge theories (2024), arXiv:2403.08892 [hep-lat].

[99] J. Osborne, I. P. McCulloch, and J. C. Halimeh, Quantum many-body scarring in $2 + 1$d gauge theories with dynamical matter (2024), arXiv:2403.08858 [cond-mat.quant-gas].

[100] J. Osborne, B. Yang, I. P. McCulloch, P. Hauke, and J. C. Halimeh, Spin-$S$U(1) Quantum Link Models with Dynamical Matter on a Quantum Simulator (2023), arXiv:2305.06368 [cond-mat.quant-gas].

[101] D. Luo, J. Shen, M. Highman, B. K. Clark, B. DeMarco, A. X. El-Khadra, and B. Gadway, A Framework for Simulating Gauge Theories with Dipolar Spin Systems (2019), arXiv:1912.11488 [quant-ph].

[102] E. Zohar and M. Burrello, Formulation of lattice gauge theories for quantum simulations, Phys. Rev. **D91**, 054506 (2015), arXiv:1409.3085 [quant-ph].

[103] E. Zohar, A. Farace, B. Reznik, and J. I. Cirac, Digital lattice gauge theories, Phys. Rev. **A95**, 023604 (2017), arXiv:1607.08121 [quant-ph].

[104] J. Bender, E. Zohar, A. Farace, and J. I. Cirac, Digital quantum simulation of lattice gauge theories in three

[105] D. C. Hackett, K. Howe, C. Hughes, W. Jay, E. T. Neil, and J. N. Simone, Digitizing Gauge Fields: Lattice Monte Carlo Results for Future Quantum Computers, Phys. Rev. A **99**, 062341 (2019), arXiv:1811.03629 [quant-ph].

[106] A. Alexandru, P. F. Bedaque, S. Harmalkar, H. Lamm, S. Lawrence, and N. C. Warrington (NuQS), Gluon field digitization for quantum computers, Phys.Rev.D **100**, 114501 (2019), arXiv:1906.11213 [hep-lat].

[107] A. Yamamoto, Real-time simulation of (2+1)-dimensional lattice gauge theory on qubits, PTEP **2021**, 013B06 (2021), arXiv:2008.11395 [hep-lat].

[108] Y. Ji, H. Lamm, and S. Zhu (NuQS), Gluon Field Digitization via Group Space Decimation for Quantum Computers, Phys. Rev. D **102**, 114513 (2020), arXiv:2005.14221 [hep-lat].

[109] J. F. Haase, L. Dellantonio, A. Celi, D. Paulson, A. Kan, K. Jansen, and C. A. Muschik, A resource efficient approach for quantum and classical simulations of gauge theories in particle physics, Quantum **5**, 393 (2021), arXiv:2006.14160 [quant-ph].

[110] M. Carena, H. Lamm, Y.-Y. Li, and W. Liu, Lattice Renormalization of Quantum Simulations (2021), arXiv:2107.01166 [hep-lat].

[111] T. Armon, S. Ashkenazi, G. García-Moreno, A. González-Tudela, and E. Zohar, Photon-mediated Stroboscopic Quantum Simulation of a $\mathbb{Z}_2$ Lattice Gauge Theory (2021), arXiv:2107.13024 [quant-ph].

[112] C. Charles, E. J. Gustafson, E. Hardt, F. Herren, N. Hogan, H. Lamm, S. Starecheski, R. S. Van de Water, and M. L. Wagman, Simulating $\mathbb{Z}_2$ lattice gauge theory on a quantum computer (2023), arXiv:2305.02361 [hep-lat].

[113] R. Irmejs, M. C. Banuls, and J. I. Cirac, Quantum simulation of Z2 lattice gauge theory with minimal resources, Phys. Rev. D **108**, 074503 (2023).

[114] E. J. Gustafson and H. Lamm, Toward quantum simulations of $\mathbb{Z}_2$ gauge theory without state preparation, Phys. Rev. D **103**, 054507 (2021), arXiv:2011.11677 [hep-lat].

[115] T. Hartung, T. Jakobs, K. Jansen, J. Ostmeyer, and C. Urbach, Digitising SU(2) gauge fields and the freezing transition, Eur. Phys. J. C **82**, 237 (2022), arXiv:2201.09625 [hep-lat].

[116] M. Creutz, L. Jacobs, and C. Rebbi, Monte Carlo Study of Abelian Lattice Gauge Theories, Phys. Rev. **D20**, 1915 (1979).

[117] M. Creutz and M. Okawa, Generalized Actions in $Z(p)$ Lattice Gauge Theory, Nucl. Phys. **B220**, 149 (1983).

[118] G. Bhanot and C. Rebbi, Monte Carlo Simulations of Lattice Models With Finite Subgroups of SU(3) as Gauge Groups, Phys. Rev. **D24**, 3319 (1981).

[119] D. Petcher and D. H. Weingarten, Monte Carlo Calculations and a Model of the Phase Structure for Gauge Theories on Discrete Subgroups of SU(2), Phys. Rev. **D22**, 2465 (1980).

[120] G. Bhanot, SU(3) Lattice Gauge Theory in Four-dimensions With a Modified Wilson Action, Phys. Lett. **108B**, 337 (1982).

[121] D. H. Weingarten and D. N. Petcher, Monte Carlo Integration for Lattice Gauge Theories with Fermions, Phys. Lett. **99B**, 333 (1981).

[122] D. Weingarten, Monte Carlo Evaluation of Hadron Masses in Lattice Gauge Theories with Fermions, Phys. Lett. **109B**, 57 (1982), [,631(1981)].

[123] Y. Ji, H. Lamm, and S. Zhu, Gluon Digitization via Character Expansion for Quantum Computers (2022), arXiv:2203.02330 [hep-lat].

[124] A. Alexandru, P. F. Bedaque, R. Brett, and H. Lamm, Spectrum of digitized QCD: Glueballs in a S(1080) gauge theory, Phys. Rev. D **105**, 114508 (2022), arXiv:2112.08482 [hep-lat].

[125] M. Carena, E. J. Gustafson, H. Lamm, Y.-Y. Li, and W. Liu, Gauge theory couplings on anisotropic lattices, Phys. Rev. D **106**, 114504 (2022), arXiv:2208.10417 [hep-lat].

[126] J. B. Kogut, 1/n Expansions and the Phase Diagram of Discrete Lattice Gauge Theories With Matter Fields, Phys. Rev. D **21**, 2316 (1980).

[127] J. Romers, *Discrete gauge theories in two spatial dimensions*, Ph.D. thesis, Master's thesis, Universiteit van Amsterdam (2007).

[128] E. H. Fradkin and S. H. Shenker, Phase Diagrams of Lattice Gauge Theories with Higgs Fields, Phys. Rev. D **19**, 3682 (1979).

[129] D. Harlow and H. Ooguri, Symmetries in quantum field theory and quantum gravity (2018), arXiv:1810.05338 [hep-th].

[130] D. Horn, M. Weinstein, and S. Yankielowicz, Hamiltonian Approach to Z(N) Lattice Gauge Theories, Phys. Rev. D **19**, 3715 (1979).

[131] B. Assi and H. Lamm, Digitization and subduction of SU(N) gauge theories, Phys. Rev. D **110**, 074511 (2024), arXiv:2405.12204 [hep-lat].

[132] T. Tilma and E. C. G. Sudarshan, Generalized Euler angle parametrization for SU(N), Journal of Physics A Mathematical General **35**, 10467 (2002), arXiv:math-ph/0205016 [math-ph].

[133] S. Bertini, S. L. Cacciatori, and B. L. Cerchiai, On the Euler angles for SU(N ), Journal of Mathematical Physics **47**, 043510 (2006), arXiv:math-ph/0510075 [math-ph].

[134] T. Tilma and E. C. G. Sudarshan, Generalized Euler angle parameterization for U( N) with applications to SU( N) coset volume measures, Journal of Geometry and Physics **52**, 263 (2004), arXiv:math-ph/0210057 [math-ph].

[135] F. S. Khan and M. Perkowski, Synthesis of multi-qudit hybrid and *d*-valued quantum logic circuits by decomposition, Theor. Comput. Sci. **367**, 336 (2006).

[136] J. R. Stryker, Oracles for Gauss's law on digital quantum computers, Phys. Rev. **A99**, 042301 (2019), arXiv:1812.01617 [quant-ph].

[137] S. Harmalkar, H. Lamm, and S. Lawrence (NuQS), Quantum Simulation of Field Theories Without State Preparation (2020), arXiv:2001.11490 [hep-lat].

[138] J. Saroni, H. Lamm, P. P. Orth, and T. Iadecola, Reconstructing thermal quantum quench dynamics from pure states, Phys. Rev. B **108**, 134301 (2023), arXiv:2307.14508 [quant-ph].

[139] A. Blais, A. L. Grimsmo, S. M. Girvin, and A. Wallraff, Circuit quantum electrodynamics, Rev. Mod. Phys. **93**, 025005 (2021), arXiv:2005.12667 [quant-ph].

[140] M. Boissonneault, J. M. Gambetta, and A. Blais, Dispersive regime of circuit QED: Photon-dependent qubit dephasing and relaxation rates, Physical Review A **79**, 10.1103/physreva.79.013819 (2009).

[141] S. Krastanov, V. V. Albert, C. Shen, C.-L. Zou, R. W.

Heeres, B. Vlastakis, R. J. Schoelkopf, and L. Jiang, Universal control of an oscillator with dispersive coupling to a qubit, Phys. Rev. A **92**, 040303 (2015).

[142] F. W. Strauch, All-resonant control of superconducting resonators, Physical Review Letters **109**, 10.1103/physrevlett.109.210501 (2012).

[143] C. K. Law and J. H. Eberly, Arbitrary control of a quantum electromagnetic field, Phys. Rev. Lett. **76**, 1055 (1996).

[144] T. F. Roque, A. A. Clerk, and H. Ribeiro, Engineering fast high-fidelity quantum operations with constrained interactions (2020), arXiv:2003.12096 [quant-ph].

[145] X. Fei, L. T. Brady, J. Larson, S. Leyffer, and S. Shen, Binary Control Pulse Optimization for Quantum Systems, Quantum **7**, 892 (2023), arXiv:2204.05773 [quant-ph].

[146] L. M. Seifert, J. Chadwick, A. Litteken, F. T. Chong, and J. M. Baker, Time-Efficient Qudit Gates through Incremental Pulse Re-seeding, in *2022 IEEE International Conference on Quantum Computing and Engineering* (2022) arXiv:2206.14975 [quant-ph].

[147] P. Luchi, F. Turro, V. Amitrano, F. Pederiva, X. Wu, K. Wendt, J. L. Dubois, and S. Quaglioni, Control optimization for parametric Hamiltonians by pulse reconstruction, Eur. Phys. J. A **59**, 196 (2023), arXiv:2102.12316 [quant-ph].

[148] A. Reineri, S. Zorzetti, T. Roy, and X. You, Exploration of superconducting multi-mode cavity architectures for quantum computing, in *2023 International Conference on Quantum Computing and Engineering* (2023) arXiv:2308.11740 [physics.app-ph].

[149] X. You *et al.*, Crosstalk-Robust Quantum Control in Multimode Bosonic Systems (2024), arXiv:2403.00275 [quant-ph].

[150] J. Job, Efficient, direct compilation of SU(N) operations into SNAP & Displacement gates (2023), arXiv:2307.11900 [quant-ph].

[151] O. Ogunkoya, J. Kim, B. Peng, A. Barış Özgüler, and Y. Alexeev, Qutrit circuits and algebraic relations: A pathway to efficient spin-1 Hamiltonian simulation, Phys. Rev. A **109**, 012426 (2024), arXiv:2309.00740 [quant-ph].

[152] P. Roy, J. van de Wetering, and L. Yeh, The Qudit ZH-Calculus: Generalised Toffoli+Hadamard and Universality, EPTCS **384**, 142 (2023), arXiv:2307.10095 [quant-ph].

[153] K. Mato, M. Ringbauer, S. Hillmich, and R. Wille, Compilation of Entangling Gates for High-Dimensional Quantum Systems, in *28th Asia and South Pacific Design Automation Conference* (2023) arXiv:2301.04155 [quant-ph].

[154] O. Ogunkoya, K. Morris, and D. M. Kürkçüoglu, Investigating Parameter Trainability in the SNAP-Displacement Protocol of a Qudit system (2023), arXiv:2309.14942 [quant-ph].

[155] B. Şahinoğlu and R. D. Somma, Hamiltonian simulation in the low energy subspace (2020), arXiv:2006.02660 [quant-ph].

[156] T. Hatomura, State-dependent error bound for digital quantum simulation of driven systems (2022), arXiv:2201.04835 [quant-ph].

[157] D. Burgarth, N. Galke, A. Hahn, and L. van Luijk, State-dependent Trotter limits and their approximations, Phys.

Rev. A **107**, L040201 (2023), arXiv:2209.14787 [quant-ph].

[158] K. Kormann, S. Holmgren, and H. Karlsson, A fourier-coefficient based solution of an optimal control problem in quantum chemistry, J. Optimization Theory and Applications **147**, 491 (2010).

[159] A. Pagano, M. M. Müller, T. Calarco, S. Montangero, and P. Rembold, The Role of Bases in Quantum Optimal Control (2024), arXiv:2405.20889 [quant-ph].

[160] N. Karjanto, Properties of chebyshev polynomials (2020), arXiv:2002.01342 [math.HO].

[161] C. Gerry and P. Knight, *Introductory Quantum Optics* (Cambridge University Press, 2004).

[162] M. S. Alam *et al.*, Quantum computing hardware for HEP algorithms and sensing, in *2022 Snowmass Summer Study* (2022) arXiv:2204.08605 [quant-ph].

[163] C. J. Axline, L. D. Burkhart, W. Pfaff, M. Zhang, K. Chou, P. Campagne-Ibarcq, P. Reinhold, L. Frunzio, S. Girvin, L. Jiang, *et al.*, On-demand quantum state transfer and entanglement between remote microwave cavity memories, Nature Physics **14**, 705 (2018).

[164] T. Fösel, S. Krastanov, F. Marquardt, and L. Jiang, Efficient cavity control with SNAP gates (2020), arXiv:2004.14256 [quant-ph].

[165] J. J. Vartiainen, M. Möttönen, and M. M. Salomaa, Efficient Decomposition of Quantum Gates, Phys. Rev. Lett. **92**, 177902 (2004).

[166] N. P. D. Sawaya, T. Menke, T. H. Kyaw, S. Johri, A. Aspuru-Guzik, and G. G. Guerreschi, Resource-efficient digital quantum simulation of d-level systems for photonic, vibrational, and spin-s Hamiltonians, npj Quantum Information **6**, 49 (2020), arXiv:1909.12847 [quant-ph].

[167] O. Di Matteo, A. McCoy, P. Gysbers, T. Miyagi, R. M. Woloshyn, and P. Navrátil, Improving Hamiltonian encodings with the Gray code, Phys. Rev. A **103**, 042405 (2021).

[168] C. C. Chang, K. S. McElvain, E. Rrapaj, and Y. Wu, Improving Schrödinger Equation Implementations with Gray Code for Adiabatic Quantum Computers (2021), arXiv:2103.08056 [quant-ph].

[169] M. G. Kendall, A new measure of rank correlation, Biometrika **30**, 81 (1938).

[170] F. J. Damerau, A technique for computer detection and correction of spelling errors, Commun. ACM **7**, 171–176 (1964).

[171] V. Levenshtein, Binary codes capable of correcting deletions, insertions, and reversals, Proceedings of the Soviet physics doklady (1966).

[172] V. V. Shende, I. L. Markov, and S. S. Bullock, Minimal universal two-qubit controlled-not-based circuits, Phys. Rev. A **69**, 062321 (2004).

[173] D. C. McKay, I. Hincks, E. J. Pritchett, M. Carroll, L. C. G. Govia, and S. T. Merkel, Benchmarking Quantum Processor Performance at Scale (2023), arXiv:2311.05933 [quant-ph].

[174] D. C. Liu and J. Nocedal, On the limited memory bfgs method for large scale optimization, Mathematical programming **45**, 503 (1989).